Rule-based modulation of a sensorimotor transformation across cortical areas

Yi-Ting Chang[1,2], Eric A. Finkel[1], Duo Xu[1,2], Daniel H. O'Connor[1,2,†]

[1]Solomon H. Snyder Department of Neuroscience, Kavli Neuroscience Discovery Institute, Brain Science Institute, Johns Hopkins University School of Medicine, Baltimore, MD

[2]Zanvyl Krieger Mind/Brain Institute, Johns Hopkins University, Baltimore, MD

[†] Correspondence: dan.oconnor@jhmi.edu

HIGHLIGHTS

- Task rules are reflected in preparatory activity in sensory and motor cortices.
- Neural subspaces for processing tactile signals depend on the current task rule.
- Motor cortical activity tracks rule switches and is required for flexible rule-guided behavior.

ABSTRACT

Flexible responses to sensory stimuli based on changing rules are critical for adapting to a dynamic environment. However, it remains unclear how the brain encodes rule information and uses this information to guide behavioral responses to sensory stimuli. Here, we made single-unit recordings while head-fixed mice performed a cross-modal sensory selection task in which they switched between two rules in different blocks of trials: licking in response to tactile stimuli applied to a whisker while rejecting visual stimuli, or licking to visual stimuli while rejecting the tactile stimuli. Along a cortical sensorimotor processing stream including the primary (S1) and secondary (S2) somatosensory areas, and the medial (MM) and anterolateral (ALM) motor areas, the single-trial activity of individual neurons distinguished between the two rules both prior to and in response to the tactile stimulus. Variable rule-dependent responses to identical stimuli could in principle occur via appropriate configuration of pre-stimulus preparatory states of a neural population, which would shape the subsequent response. We hypothesized that neural populations in S1, S2, MM and ALM would show preparatory activity states that were set in a rule-dependent manner to cause processing of sensory information according to the current rule. This hypothesis was supported for the motor cortical areas by findings that (1) the current task rule could be decoded from pre-stimulus population activity in ALM and MM; (2) neural subspaces containing the population activity differed between the two rules both prior to the stimulus and during the stimulus-evoked response; and (3) optogenetic disruption of pre-stimulus states within ALM and MM impaired task performance. Our findings indicate that flexible selection of an appropriate action in response to a sensory input can occur via configuration of preparatory states in the motor cortex.

INTRODUCTION

Abstract relationships between objects, events, and actions can be established by rules. How we receive, process, and respond to sensory signals is guided by our understanding of rules that apply to the current context. For example, a student picks up a vibrating phone while

waiting for a phone interview, but not during a lecture. This rule-guided flexibility is essential to adapt in a dynamic environment[1] and is at the core of many advanced cognitive functions such as economic decision making and social interaction[2,3]. Several lines of studies have shown that impairments in rule-based decision making are linked to neurodevelopmental conditions including autism spectrum disorder[4,5] and schizophrenia[6,7].

Flexible rule-guided behaviors require at least two processes from the brain. First, (#1) to maintain and update rule representations; and (#2) to apply the appropriate rule to correctly transform sensory signals into motor outputs. Higher-order brain areas in frontal and parietal cortices are thought to play an important role in process #1, that is in encoding abstract rules and guiding the sensorimotor transformation[1,8–12]. It remains less clear how process #2 occurs, i.e. how rules are applied to sensorimotor pathways to govern the mapping between stimulus and response[13].

Rodent orofacial circuits provide well-defined sensorimotor pathways to study rule implementation. Recent studies have uncovered important cortical areas linking whisker input to licking output in goal-directed behavior[14–17]. For example, findings in a delayed tactile detection task have shown that the whisker region of primary somatosensory cortex is required for sensory detection and the anterior lateral motor cortex (ALM) is critical for motor planning and execution of licking[15,18]. Additionally, the medial motor cortex (MM), which contains the whisker primary and secondary motor cortices[19,20], demonstrates early selectivity of whisker-based tactile signals compared with ALM[21].

Activity in sensorimotor pathways can reflect both sensory input and the rules dictating the appropriate use of that input[11,13,22–24]. Analysis of neural populations may provide insight into how these sensory and contextual signals are integrated to govern behavior. Recent progress in the study of neural population dynamics has uncovered population-level computations for motor control[25–28], timing[29–31] and decision-making[32–35]. The evolution of the neural population state is controlled by initial conditions, internal dynamics, and external inputs, and can allow computations to be carried out[36]. For example, preparatory activity in non-human primate motor and premotor areas has been proposed to initialize dynamical systems to generate appropriate arm movements[37,38]. In addition, thalamic input has been shown to drive cortical dynamics in the mouse motor cortex during reaching[28]. In the primate dorsomedial frontal cortex, the speed of neural trajectories encoding the passage of time is adjusted by both initial conditions and thalamic inputs[30,31].

Here we investigate how task rules affect activity in a sensorimotor pathway to govern the mapping between stimulus and response. We trained mice in a cross-modal sensory selection task that we recently developed[39] and then recorded and analyzed population single-unit activity from a set of cortical areas along the pathway that transforms whisker sensory inputs into licking motor outputs[15,18,21]. We found that single-neuron and population activity before stimulus delivery reflected task rules in the whisker regions of primary (S1) and secondary (S2) somatosensory cortical areas, and in the medial (MM) and anterolateral (ALM) motor cortical areas. Across these cortical areas, neural subspaces containing the trial activity differed between the two

rules, including during a pre-stimulus period. Pre-stimulus population states in the motor cortical areas shifted in a manner that tracked the rule switch. Optogenetic inhibition designed to disrupt pre-stimulus states in the motor cortical areas impaired rule-dependent tactile detection. Together, our results show that the application of task rules—to link a stimulus to the correct response—involves rule-dependent configuration of pre-stimulus preparatory states within the sensorimotor cortex.

RESULTS

Task rules modulate touch-evoked activity of individual neurons in the tactile processing stream

We trained head-fixed mice to perform a cross-modal sensory selection task[39] in which they switched between “respond-to-touch” and “respond-to-light” rules in different blocks of trials (Fig. 1a,b). During the respond-to-touch rule, mice responded to a tactile stimulus by licking to the right reward port, and to withhold licking following a visual stimulus. During the respond-to-light rule, mice responded to a visual stimulus by licking to the left reward port, and withheld licking following a tactile stimulus. Blocks of trials under the two rules alternated multiple times in a session (Fig. 1b; 4-6 blocks per session, ~60 trials per block). No cue was immediately provided after rule switching, so mice detected the rule change through reward availability over the first few trials. On the 9th trial, a drop of water from the correct reward port was released following the stimulus to ensure switching (Fig. 1b, black dots).

The two stimulus-response rules determined the behavioral relevance of sensory stimuli. For example, tactile stimuli were behaviorally relevant in respond-to-touch blocks but irrelevant in respond-to-light blocks. Four trial outcomes were defined based on the behavioral relevance of a sensory stimulus and on the response of the mouse. Correct licking responses following a relevant stimulus were “hits”, and correct withholding of responses following an irrelevant stimulus were “correct rejections”. Failed responses to a relevant stimulus were “misses”, and incorrect licking responses (following an irrelevant stimulus and/or at the incorrect port) were “false alarms”. Two sensory modalities and four trial outcomes composed eight trial types in the cross-modal sensory selection task (Fig. 1c). Only hit trials were rewarded with a drop of water, and the other trial types were neither rewarded nor punished. We used stimulus strengths (tactile stimulus: single whisker, 20 Hz, 150 ms, ~800° s^{-1}; visual stimulus: 470 nm LED, 150 ms, ~3 μW) that yielded performance of approximately 75% correct for both respond-to-touch and respond-to-light blocks (Fig. 1d; touch: 74 ± 1%, light: 75 ± 1% (mean ± sem), $p = 0.56$, paired sample t-test, n = 12 mice). Thus, mice flexibly responded to tactile and visual stimuli in a rule-dependent manner.

To examine how the task rules influenced the sensorimotor transformation occurring in the tactile processing stream, we performed single-unit recordings from sensory and motor cortical areas including S1, S2, MM and ALM using 64-channel silicon probes (Fig. 1e-g and Fig. S1a-h). In tactile stimulus trials, some neurons in sensory and motor cortical areas showed prominent touch-evoked responses in both block types (e.g. Fig. S1c). Most of these touch-evoked responses appeared enhanced and sustained at timepoints prior to licking in the

respond-to-touch (tactile hit, “tHit”) blocks when compared with similar timepoints in the respond-to-light (tactile correct rejection, “tCR”) blocks (Fig.1f and Fig. S1a,e). In contrast, some neurons only showed increased activity when mice made lick responses, regardless of the block type (Fig. S1d,f,h). Neurons could also show a mixture of these two response types (Fig. S1b,g).

We first determined to what extent the rules modulated touch-evoked activity by comparing tactile correct trials between respond-to-touch and respond-to-light blocks (tHit vs tCR). We restricted analysis to the 150 ms period of stimulus delivery, to focus on rule-dependent processing that was not influenced by overt movements (97% of lick onsets occurred >150 ms after stimulus onset). We used ideal observer analysis to determine how well trial-by-trial activity of a single neuron could discriminate between the task rules. We found that 8-16% of neurons in these cortical areas had area under the receiver-operating curve (AUC) values significantly different from 0.5, and therefore discriminated between tHit and tCR trials (Fig. 1h; S1: 11.9%, n = 177; S2: 8%, n = 162; MM: 16.4%, n = 140; ALM: 12.1%, n = 256; criterion to be considered significant: Bonferroni corrected 95% CI on AUC did not include 0.5). Moreover, the distribution of AUC values for discriminative neurons showed that the majority had enhanced responses (AUC > 0.5) to tactile stimuli that were behaviorally relevant. Therefore, touch-evoked responses were overall enhanced by the relevance of tactile stimuli according to the current stimulus-response rule.

Pre-stimulus activity of single neurons signals task rules

In our cross-modal selection task, rules were block-based and there were no cues to indicate the current rule (except for the rule transition cue on the 9th trial of each block), so the mice were required to maintain rule information during the inter-trial interval (ITI). To test if ITI activity of neurons in the somatosensory and motor cortical areas reflected task rules, we first analyzed neural activity during the one second window preceding stimulus delivery. Trials with licking in this time window were removed to minimize possible movement effects on pre-stimulus activity (Methods). We found that some cortical neurons showed obvious changes in their pre-stimulus activity across blocks (Fig. 2a). A preference for the respond-to-touch rule (that is, with activity higher in respond-to-touch blocks compared with respond-to-light blocks) and a preference for the respond-to-light rule were both observed (Fig. 2a,b). We next calculated discriminability between block types for each neuron to see how well an ideal observer could categorize the current trial’s task rule on the basis of pre-stimulus activity (-100 to 0 ms from stimulus onset). To ensure mice were in the correct state to treat the following stimuli according to the rule, only correct tactile and visual trials were included. Less than 5% of neurons in S1 and S2 showed significant rule discriminability, while MM and ALM had around 10-20% significant neurons (Fig. 2c; S1: 4.5%, n= 177; S2: 2.5%, n= 162; MM: 21.4%, n= 140; ALM: 10.2%, n= 256; Bonferroni corrected 95% CI on AUC did not include 0.5).

We also calculated the ability of each neuron to discriminate between tactile vs visual stimuli in windows before (-100 to 0 ms) or after (0 to 100 ms) stimulus onset, to serve as negative and positive controls, respectively, for our use of ideal observer analysis. As expected, single-unit activity before stimulus onset did not discriminate between tactile and visual trials (Fig. 2d; S1: 0%; S2: 0%; MM: 0%; ALM: 0.8%). After stimulus onset, more than 35% of neurons in the

sensory cortical areas and approximately 15% of neurons in the motor cortical areas showed significant stimulus discriminability (Fig. 2e; S1: 37.3%; S2: 35.2%; MM: 15%; ALM: 14.1%).

The rule dependence of pre-stimulus activity indicates that neurons were in different states immediately prior to stimulus onset, suggesting that their responses to the subsequent sensory input might also differ. We therefore next investigated early touch-evoked responses (0 to 50 ms from stimulus onset) in those neurons that showed significant rule discriminability prior to stimulus delivery. We found that neurons with stronger preference for the respond-to-touch rule before stimulus onset showed larger touch-evoked activity in the respond-to-touch blocks, whereas neurons with a preference for the respond-to-light rule showed larger touch-evoked activity in the respond-to-light blocks (Fig. 2f; Pearson correlation; S1: $r = 0.69$, $p = 0.056$, 8 neurons; S2: $r = 0.91$, $p = 0.093$, 4 neurons; MM: $r = 0.93$, $p < 0.001$, 30 neurons; ALM: $r = 0.83$, $p < 0.001$, 26 neurons). This result suggests that configuration of pre-stimulus states could play a role in achieving rule dependence of sensory processing.

Together, these results demonstrate that the pre-stimulus activity of single units in the sensory and motor cortical areas reflected task rules, with better discrimination of rules by units in the motor areas.

Pre-stimulus states of neuronal populations reflect task rules

We next investigated the function of rule-dependent pre-stimulus activity from the perspective of neural population dynamics. In a dynamical system, state variables change based on their current values. This implies that the evolution of neural population activity during a trial will depend in part on the activity state of the population at the beginning of the trial[36,40]. We hypothesized that pre-stimulus activity—i.e. the state of the population at the start of the trial—would be set in such a way as to enable processing of the upcoming sensory signals according to the appropriate rule. Predictions from this hypothesis are that: (1) the pre-stimulus state of a neural population could be used to decode the current task rule; (2) the rule-dependent separation of neural subspaces before and after the tactile stimulus onset should be correlated; (3) pre-stimulus states would shift when the mice switched between rules; and (4) perturbations of the pre-stimulus state should disrupt task performance. We tested each prediction via the following analyses and experiments.

We first determined whether the pre-stimulus population state could be used to decode the current task rule. For each session, we used linear discriminant analysis (LDA) to obtain a classification accuracy for block type (respond-to-touch vs respond-to-light) based on the pre-stimulus activity (-100 to 0 ms relative to stimulus onset) of simultaneously recorded neurons on correct trials (Fig. 3a). Pre-stimulus states in S1, S2, MM and ALM could each be used to decode the block type (Fig. 3b; medians of classification accuracy [true vs shuffled]: S1 [0.61 vs 0.5], 10 sessions; S2 [0.62 vs 0.53], 8 sessions; MM [0.7 vs 0.52], 9 sessions; ALM [0.68 vs 0.55], 13 sessions). Support vector machine (SVM) and Random Forest classifiers showed similar decoding abilities (Fig. S2a,b; medians of classification accuracy [true vs shuffled]; SVM: S1 [0.6 vs 0.53], S2 [0.61 vs 0.51], MM [0.71 vs 0.51], ALM [0.65 vs 0.52]; Random Forests: S1 [0.59 vs 0.52], S2 [0.6 vs 0.52], MM [0.65 vs 0.49], ALM [0.7 vs 0.5]).

Interestingly, activity in the motor cortical areas allowed robust block-type classification (no overlap between bootstrap 95% CIs for the true and shuffled data, 95% CIs for true vs shuffled data: MM [0.60,0.73] vs [0.48, 0.53]; ALM [0.56,0.66] vs [0.49, 0.54]). In contrast, the sensory cortical areas showed limited block-type discriminability (Fig. 3c; bootstrap 95% CIs for the true data were above 0.5 but overlapped with the bootstrap 95% CIs for the shuffled data, 95% CIs for true vs shuffled data: S1 [0.52,0.61] vs [0.49,0.55]; S2 [0.53,0.63] vs [0.49, 0.54]). In positive and negative control analyses, we found that neural population activity could be used to discriminate between stimulus types (tactile vs visual) after stimulus onset (Fig. 3e and Fig. S2d; 0 to 100 ms relative to stimulus onset) but not before stimulus onset (Fig. 3d and Fig. S2c; from -100 to 0 ms).

Together these results show that each of the two task rules was associated with a different pattern of pre-stimulus population activity in sensory and motor cortical areas, with a larger difference in the motor areas.

Separation of pre-stimulus states predicts subsequent divergent processing

We found pre-stimulus population activity was rule-dependent across sensory and motor cortical areas. We next asked if these rule-dependent pre-stimulus states affect post-stimulus neural activity. We investigated the relationship between the difference in pre-stimulus states between tHits and tCRs and the divergence of their subsequent neural trajectories. To assess this for the four cortical areas, we quantified how the tHit and tCR trajectories diverged from each other by calculating the Euclidean distance between matching time points for all possible pairs of tHit and tCR trajectories for a given session and then averaging these for the session (Fig. 4a,b; window of analysis: -100 to 150 ms relative to stimulus onset; 10 ms bins; using the top 3 PCs; Methods). The resulting time series of distance values from all sessions (n = 40) were then ranked according to their means over the 100 ms period preceding stimulus onset and split into two groups, those above and below the median. The top 50% group showed a larger mean distance between tHit and tCR trajectories after stimulus onset compared with the bottom 50% group[41,42] (Fig. 4c; $p < 0.001$, permutation test). This result shows that the difference in population responses to the tactile stimuli under the two rules is commensurate with the difference in pre-stimulus states.

Neural subspaces for tactile processing are rule-dependent

Although the full dimensionality of a neural state space is equal to the number of neurons, correlations among neurons typically cause dynamics to occur within a subspace of lower dimensionality[40,43]. Population activity associated with each task rule might not only follow distinct trajectories, but could also occur within different neural subspaces. To test this, we calculated the overlap between the subspaces associated with tHit and tCR trials[35,44,45] (Fig. 4d; see Methods). We expect that, if tHit and tCR trial activity occupies largely overlapping subspaces, then the neural dimensions capturing most of the tHit activity will also explain much of the tCR activity (Fig. 4d, middle). Conversely, if they occupy largely distinct subspaces, then the dimensions capturing most of the tHit activity will explain little of the tCR activity (Fig. 4d, right). For each session, tHit trials were divided randomly into equally-sized “reference” and “control” groups. The reference tHit trials were then used to perform a principal component

analysis (PCA; using data 0 to 150 ms from stimulus onset; 10 ms bins). We projected activity from tCR trials and from the control tHit trials into the space of the top-three principal components obtained from the reference group PCA, then calculated and normalized their variance explained (Methods; using data 0 to 150 ms from stimulus onset). For S1, S2, MM and ALM, subspace overlaps for tCR trials were significantly lower than the corresponding subspace overlaps for the control tHit trials (Fig. 4e, dark purple vs gray symbols; tCR – control tHit: S1 [-0.23], 8 sessions, $p = 0.0016$; S2 [-0.23], 7 sessions, $p = 0.0086$; MM [-0.36], 5 sessions, $p = <0.001$; ALM [-0.35], 11 sessions, $p < 0.001$, paired-t test). This finding suggests that different neural subspaces were used for processing tactile stimuli under each of the two rules, in both sensory and motor cortical areas.

We next asked if the rule-dependent separation of subspaces we observed began prior to the tactile stimulus. This would provide evidence that differences in tactile stimulus processing follow from differences in the state of the neural population at the time the stimulus is received. We found that subspace overlaps for tCR trials before stimulus onset (from -100 to 0 ms) were significantly lower than the subspace overlaps for the control tHit trials (Fig. 4e, light purple vs gray symbols; pre-stimulus-onset tCR – control tHit: S1 [-0.28], $p = 0.001$; S2 [-0.31], $p < 0.001$; MM [-0.38], $p < 0.001$; ALM [-0.33], $p < 0.001$, paired-t test). Moreover, across the cortical areas, the subspace overlaps for tCR trials calculated from periods before and after the tactile stimulus onset were correlated (Fig. 4f; Pearson correlation, $r = 0.68$, $p < 0.001$; 31 sessions). This indicates that the shift between neural subspaces associated with each rule occurred prior to stimulus delivery and should thus impact processing of the stimulus.

Together, our results suggest that cortical populations are “pre-configured” according to the current rule, such that an incoming sensory signal leads to distinct processing and ultimately distinct actions.

Choice coding dimensions change with task rule

Gating of sensory information involves changing how sensory information is represented and read out[32]. This can be achieved by shifting sensory and/or choice coding dimensions in the population activity space[34,46]. In the previous section, we showed that neural subspaces containing trial dynamics changed between the two task rules. We next asked whether stimulus and choice coding dimensions within these subspaces also shifted with task rules. For each task rule, we estimated coding dimensions (CDs) that maximally discriminated the neural trajectories for different conditions[47,48] (Fig. S3a-d; Methods). Since mice rarely licked the wrong port for a given block (Fig. 1b), right-lick and no-lick trials were used to obtain choice coding dimensions for the respond-to-touch blocks, and left-lick and no-lick trials for the respond-to-light blocks. To assess whether stimulus and choice CDs changed with task rule, we calculated for each session the dot product between the CDs obtained from respond-to-touch and respond-to-light blocks. We then used the magnitude of this dot product as an unsigned measure of the relative orientations of the CDs. In ALM, the dot product magnitudes calculated between stimulus CDs for the two block types were not significantly different from those calculated after shuffling trial-type labels (Fig. S3e; significance defined as non-overlap of 95% CIs). This suggests that the stimulus CD in a respond-to-touch block had an orientation

unrelated to that in a respond-to-light block. In contrast, we found that S1, S2 and MM had stimulus CDs that were significantly aligned between the two block types (Fig. S3e; magnitude of dot product between the respond-to-touch stimulus CDs and the respond-to-light stimulus CDs, mean ± 95% CI for true vs shuffled data: S1: 0.5 ± [0.34, 0.66] vs 0.21 ± [0.12, 0.34]; S2: 0.62 ± [0.43, 0.78] vs 0.22 ± [0.13, 0.31]; MM: 0.48 ± [0.38, 0.59] vs 0.24 ± [0.16, 0.33]; ALM: 0.33 ± [0.2, 0.47] vs 0.21 ± [0.13, 0.31]). In contrast, the choice CDs for the two block types were not aligned well in S1, S2, MM, or ALM (Fig. S3f; magnitude of dot product between the respond-to-touch choice CD and the respond-to-light choice CD, mean ± 95% CI for true vs shuffled data: S1: 0.28 ± [0.15, 0.43] vs 0.21 ± [0.12, 0.33]; S2: 0.22 ± [0.11, 0.33] vs 0.21 ± [0.13, 0.32]; MM: 0.22 ± [0.13, 0.33] vs 0.22 ± [0.14, 0.3]; ALM: 0.27 ± [0.16, 0.39] vs 0.21 ± [0.13, 0.31]). These results suggest that the different subspaces for tactile processing under the two rules result at least in part from changes in choice coding dimensions.

Pre-stimulus states in motor cortex track behavioral rule switches

Task rules switched multiple (3-5) times in each behavioral session. Mice detected a rule switch either through trial and error during the first few trials after the switch, or when a drop of water from the correct reward port was given on the 9th trial (which served as a cue to ensure that mice switched by this point; Fig. 1b). We used the first hit trial as the mark of a successful behavioral switch and found that mice switched before or immediately after the cue (Fig. 5a). To analyze how pre-stimulus states changed over the course of a rule transition, we defined a “transition period” that spanned from the first trial after a block switch until the first hit trial of the new block. In addition, we divided each transition period into “early” and “late” parts based on the occurrence of the first false alarm trial of the new block (Fig. 5b). We considered the first false alarm trial to be the point at which the mouse first received feedback to indicate that a block change had occurred.

We hypothesized that the behavioral change that marked a successful switch in rule application would be accompanied by a neural change. Specifically, that the pre-stimulus population state would progress from that typical of the prior type of block to that typical of the new type of block in parallel with the behavioral shift. To test this, we trained an LDA classifier to discriminate respond-to-touch block and respond-to-light block trials using pre-stimulus neural activity. We used 90% of the correct trials as training data and tested classifier performance on the held-out 10% of correct trials (Fig. 5c,d). Using our “transition period” definition as described above, we tested classifier performance on “early” transition and “late” transition trials (Fig. 5b). For respond-to-touch to respond-to-light block transitions, the fractions of trials classified as respond-to-touch for MM and ALM decreased progressively over the course of the transition (Fig. 5c; rank correlation of the fractions calculated for each of the separate periods spanning the transition, Kendall’s tau, mean ± 95% CI: MM: -0.39 ± [-0.67, -0.11], ALM: -0.29 ± [-0.54, -0.04]). Similarly, the fractions of trials classified as respond-to-touch increased progressively over the course of transitions from respond-to-light to respond-to-touch blocks (Fig. 5d; Kendall’s tau, mean ± 95% CI: MM: 0.37 ± [0.07, 0.63], ALM: 0.27 ± [0.03, 0.49]). Accuracies for classification of trials by block type based on S1 and S2 activity were uniformly poor and showed no clear trends across block transitions (Fig. S4; mean ± 95% CI on Kendall’s tau for respond-to-touch → respond-to-light transitions: S1: -0.16 ± [-0.43, 0.1], S2: -0.15 ± [-0.54,

0.21]; for respond-to-light → respond-to-touch transitions: S1: 0.21 ± [-0.07, 0.5], S2: 0.25 ± [-0.17, 0.63]). Together, these results indicate that the pre-stimulus states of neural populations in MM and ALM shifted over the course of block transitions in a manner commensurate with the behavioral shift in rule application.

Disruption of pre-stimulus motor cortical state impairs rule-dependent tactile detection

So far, we have shown that pre-stimulus neural population states in the sensory and motor cortical areas differed between the two task rules. This suggests that pre-stimulus activity may play a critical role in our task. To test this, we bilaterally inhibited the different cortical areas shortly before stimulus onset via optogenetic activation of parvalbumin-positive (PV) GABAergic neurons[18,49] (Fig. 6a, middle panel; -0.8 to 0 seconds from stimulus onset). Additionally, we included two other areas of the dorsal cortex, the anteromedial part of the motor cortex (AMM) and the posterior parietal cortex (PPC). We also performed negative control (sham) sessions that were identical except that the optogenetic light path was obstructed.

We defined detection sensitivity for tactile stimuli as the difference between tactile hit rate and visual false alarm rate during the response-to-touch blocks. Tactile detection sensitivity was significantly decreased when MM and ALM but not S1 and S2 were inhibited during the pre-stimulus period (Fig. 6c; criterion to be considered significant: 95% CI on Δ tactile sensitivity did not include 0; S1/S2: [-0.47, 0.08], 4 mice, 10 sessions; MM: [-0.65, -0.12], 4 mice, 11 sessions; ALM: [-0.68, -0.02], 4 mice, 10 sessions). This was primarily due to a reduction in the tactile hit rate (Fig. S5b; 95% CI on Δ tactile hit rate: S1/S2 [-0.31, 0.01]; MM [-0.49, -0.15]; ALM [-0.46, -0.07]). Inhibition of S1, S2, MM, and ALM during a 2-second window starting at the time of the stimulus onset served as a positive control (Fig. 6a, right panel). Consistent with previous studies[18,50], inhibition of these cortical areas after stimulus onset reduced detection sensitivity for tactile stimuli (Fig. 6d; 95% CI on Δ tactile sensitivity: S1/S2 [-0.67, -0.08]; MM [-0.6, -0.34]; ALM [-0.55, -0.27]). Neither the negative control (sham) condition, nor inhibition of AMM before stimulus onset, showed an effect on the detection sensitivity for tactile stimuli (Fig. 6c; sham: [-0.12, 0.13], 7 mice, 28 sessions; AMM [-0.19, 0.06], 7 mice, 21 sessions). Together, our results suggest that the pre-stimulus network activity states in MM and ALM play an important role in rule-dependent tactile processing.

We defined detection sensitivity for visual stimuli as the difference between visual hit rate and tactile false alarm rate during the respond-to-light blocks. Visual detection sensitivity was not affected when S1 and S2 were inhibited before (Fig. S6g; 95% CI on Δ visual sensitivity: [-0.27, 0.05]) or after (Fig. S6h; [-0.44, 0.04]) the stimulus onset. For pre-stimulus-onset inhibition of the motor cortical areas, visual detection sensitivity was decreased when MM and AMM but not ALM were suppressed (Fig. S6g; MM [-0.6, -0.18]; ALM [-0.5, 0.04]; AMM [-0.35, -0.08]). Inhibition of any of the three motor cortical areas after stimulus onset caused a reduction in visual sensitivity (Fig. S6h; MM [-0.83., -0.52]; ALM [-0.84, -0.39]; AMM [-0.72, -0.36]). Together, these results indicate that pre-stimulus states of neural populations in the medial parts of motor cortex, such as MM and AMM, are critical for processing visual stimuli in a rule-dependent manner.

PPC is involved in multisensory processing[51–53] and decision-making[54–58]. Here we tested for a critical role of PPC in our cross-modal selection task (7 mice, 21 sessions total). Detection sensitivities for both tactile and visual stimuli were decreased when PPC was inhibited before (Fig. 6c; Δ tactile sensitivity: [-0.4, -0.06]; Fig. S6g; Δ visual sensitivity [-0.31, -0.05]) or after the stimulus onset (Fig. 6d; Δ tactile sensitivity: [-0.43, -0.04]; Fig. S6h; Δ visual sensitivity: [-0.54, -0.07]). These reductions in tactile and visual detection sensitivities were caused by a decrease in hit rate and/or an increase in false alarm rate. In general, inhibition of PPC before stimulus onset decreased the hit rate (Fig. S5b; Δ tactile hit [-0.36, -0.05]; Fig. S6b; Δ visual hit [-0.26, 0]), whereas inhibition of PPC after stimulus onset increased the false alarm rate (Fig. S5f; Δ visual false alarm [0.13, 0.38]; Fig. S6f; Δ tactile false alarm [0, 0.25]).

It is possible that disruption of pre-stimulus states may affect aspects of tactile sensory processing and/or lick production that are unrelated to rules. To exclude this possibility, in a new cohort of mice (n = 5), we inhibited each cortical area in either the pre- or the post-stimulus-onset period during performance of a simple tactile detection task (Fig. 6e-g). In this task, mice had only to report with Go/NoGo licking whether a whisker was deflected, without rule-switching components to the task or the need to suppress responses to distracting stimuli. We found that tactile sensitivity was decreased when the sensory and motor cortical areas were inhibited after but not before stimulus onset (Fig. 6f,g; 95% CI on Δ tactile sensitivity for pre-stimulus-onset inhibition: S1/S2 [-0.34, 0.18], 3 mice, 3 sessions; MM [-0.23, 0.06], 3 mice, 5 sessions; ALM [-0.28, 0.07], 3 mice, 4 sessions; Δ tactile sensitivity for post-stimulus-onset inhibition: S1/S2 [-0.59, -0.31]; MM [-0.59, -0.25]; ALM [-0.45, -0.1]). This was mainly caused by the decrease in hit rate in the post-stimulus-onset inhibition (Fig. S5i; 95% CI on Δ tactile hit rate: S1/S2 [-0.61, -0.28]; MM [-0.67, -0.2]; ALM [-0.73, -0.05]). Inhibition of AMM and PPC did not influence tactile sensitivity in either inhibition condition (Fig. 6f,g; Δ tactile sensitivity for pre-stimulus-onset inhibition: AMM [-0.25, 0.16], 3 mice, 4 sessions; PPC [-0.12, 0.1], 3 mice, 4 sessions; Δ tactile sensitivity for post-stimulus-onset inhibition: AMM [-0.17, 0.18]; PPC [-0.14, 0.3]). Together, these results show that inhibition immediately prior to stimulus delivery did not impact the performance of a simple tactile detection task in which the stimulus-response rule remained fixed.

We conducted an additional analysis to rule out the possibility that the behavioral effects of cortical inhibition we observed could be due simply to a deficit in lick production per se. Specifically, we compared the probability of licking in laser-only trials (catch trials where there was no sensory stimulus) with the probability of licking during intertrial intervals, for both the cross-modal selection task and the simple tactile detection task (Fig. 6h). Lick probability was unaffected during S1, S2, MM and ALM experiments for both tasks, indicating that the behavioral effects were not due to an inability to lick (Fig. 6i, j; 95% CI on Δ lick probability for cross-modal selection task: S1/S2 [-0.18, 0.24]; MM [-0.31, 0.03]; ALM [-0.24, 0.16]; Δ lick probability for simple tactile detection task: S1/S2 [-0.13, 0.31]; MM [-0.06, 0.45]; ALM [-0.18, 0.34]).

Taken together, our results suggest that the pre-stimulus states of motor cortical networks play an important role in rule-dependent sensorimotor transformations.

DISCUSSION

Here we investigated how rules modulate the transformation of tactile signals into actions across a set of key sensory-motor cortical areas comprising S1, S2, MM and ALM. We found that neural activity prior to stimulus delivery reflected task rules at both the single-neuron and population levels in each area, but more prominently so in the motor cortical areas MM and ALM. Across the areas examined, each of the two task rules was associated with its own neural subspace for processing tactile signals. In ALM and MM, pre-stimulus population states shifted concomitantly with the behavioral signs of a rule switch. Optogenetic inhibition of motor cortical areas during the pre-stimulus period impaired tactile detection during the cross-modal selection task, but not during a simpler tactile detection task that did not require switching among rules. Together, our results suggest that the neural population states in motor cortical areas ALM and MM play an important role in transforming sensory stimuli into actions in a flexible, rule-dependent manner.

The responses to tactile stimuli were enhanced in S1, S2, MM and ALM when they were behaviorally relevant according to the current rule (Fig. 1h). In our task, relevance relates to reward, movement preparation, and movement, factors known to influence activity across many brain areas[21,23,59–62]. We chose not to attempt to dissociate “relevance” from these factors in our task design, given that they are linked in many natural scenarios[63,64]. Below we address potential concerns and confounding effects associated with reward and movement.

First, neural responses on tactile hits and tactile false alarms were similar, despite the fact that hits but not false alarms were rewarded (proportions of neurons showing a significant difference in mean response between tactile hits and tactile false alarms: S1 (0/177); S2 (2/162); MM (0/140); ALM (6/256); permutation tests on PSTHs with Bonferroni correction for multiple comparisons; Methods). Second, we minimized movement effects by limiting the analysis window to a period that preceded 97% of lick onsets (0 to 150 ms from stimulus onset). We also included censor and grace periods (Methods) to reduce the impact of compulsive licking, and excluded trials with licking during the one second window preceding stimuli. We note that motor-related signals need not always occur together with overt movement. For instance subthreshold stimulation of the frontal eye fields in primates can drive V4 activity and mimic the effects of attention without causing eye movements[65,66].

Responses to tactile stimuli within a respond-to-light block were significantly reduced but still observable in ALM (Fig. 1g and Fig. S1g). This suggests that gating of tactile information likely occurred in part prior to ALM[67–69]. In contrast, we did not observe visually-evoked activity in ALM (Fig. 1g and Fig. S1g-h). This modality bias is consistent with the long-range connectivity between sensory and frontal areas. Specifically, the somatosensory cortex is connected to the motor cortex, whereas the visual cortex is connected to the anterior cingulate cortex (ACC) [70]. Also consistent with this anatomy is that we observed visually-evoked activity in the anterior part of the ACC (Fig. S1i-k; the anteromedial part of the motor cortex, AMM), and ACC has been shown to modulate V1 activity in rodents[24].

In our task, the right or left water port was the rewarded port in a respond-to-touch block or a respond-to-light block, respectively. Although the mice could not anticipate stimulus types and licking responses during the intertrial interval, there might be a subtle bias of posture and movement across blocks given the different positions of the rewarded port. To reduce the effects of movement bias on pre-stimulus activity (-100 to 0 ms), we removed trials with licking during a one second window before stimulus onset. Moreover, in a separate study using the same task (Finkel et al., unpublished), high-speed video analysis demonstrated no significant differences in whisker motion between respond-to-touch and respond-to-light blocks in most (12 of 14) behavioral sessions.

We found that the neural subspaces containing population activity patterns were different during respond-to-touch and respond-to-light rules. Specifically, S1, S2, MM, and ALM showed lower subspace overlaps when calculated between tactile hits and tactile correct rejections than when calculated between tactile hits and control (held-out) tactile hits (Fig. 4e). These subspace differences could result from: (1) involvement of different sets of neurons; (2) differently signed changes in firing patterns (such as some neurons fire more and others fire less); and/or (3) differently scaled changes in firing patterns (such as the firing rates of some neurons do not change and the firing rates of other neurons increased two-fold).

We found that how well neural subspaces were separated during tactile processing was associated with how well they were separated prior to the stimulus (Fig. 4f). This result is consistent with a dynamical systems view of neural population processing, where initial conditions are of critical importance[36,38]. Bringing the population activity to an optimal initial state could allow the evolution of the population activity to produce the desired movement. Primate studies have shown that motor cortical areas implement this strategy to control movement[25,37,71]. Here we identified a potentially similar role for motor cortex activity states in the transformation of incoming sensory signals into actions in a rule-dependent manner. In addition, we found that not only motor but also sensory cortical areas had initial states that varied with the current rule. Indeed, pre-stimulus activity has been shown to encode rule information in primate visual cortex [72] and rodent auditory cortex[11]. Overall, these findings indicate that setting up appropriate initial states could be a general strategy by which cortical networks integrate external inputs to achieve context-specific processing.

Inhibition of the motor cortical areas prior to stimulus delivery slightly but significantly impaired tactile detection in the respond-to-touch rule and visual detection in the respond-to-light rule (Fig. 6c and Fig. S6g). However, the ability to detect sensory stimuli was not completely abolished. This suggests that circuits for encoding the task rules may be redundant and/or other gating mechanisms may be involved[8]. Indeed, the pre-stimulus activity in either MM and ALM could be used to decode the task rules, although we inhibited only one area at a time. Additionally, it has been shown that loops between ALM and subcortical regions including thalamus and cerebellum maintain persistent activity during short-term memory[33,73]. It is possible that recurrent circuits across multiple brain areas contribute to holding rule information during intertrial intervals.

To test for a rule-specific function of pre-stimulus states, we used a simple tactile detection task to assess the potential effects of inhibition on sensory processing and lick production (Fig. 6e-g). We found that inhibition of the pre-stimulus states of MM and ALM only reduced the detection sensitivity for tactile stimuli in the cross-modal selection task but not in the simple tactile detection task (Fig. 6c,f), suggesting a role specific to flexible rule-dependent sensorimotor transformations. We balanced the behavioral performances in these tasks (~75% correct) via the adjustment of stimulus intensity to make the task difficulties similar. However, the effects of silencing cortex can also depend on factors that we did not probe, such as the time course of an area's task involvement[74].

Pre-stimulus activity in MM and ALM showed a strong dependence on the current rule (Figs. 2,3,5), correlated with aspects of subsequent tactile processing (Fig. 4), and was required for tactile detection during the cross-modal selection task (Fig. 6c). These motor cortical areas are therefore likely to play an important role in the rule-dependent sensorimotor transformations occurring within cortical networks[75]. A greater rule-dependence of activity in motor compared with sensory areas is consistent with primate visual and somatosensory studies showing that attention effects become more prominent in higher-order areas[76–78]. Moreover, a number of studies in primates and rodents have shown that sensory-related responses in sensory cortical areas are modulated by motor cortical areas[16,63,65,79,80]. It is possible that MM and ALM received rule information from other brain regions such as the medial prefrontal cortex[8,73,81,82] and send this information to S1 and S2 in the cross-modal selection task. Future work is needed to identify and characterize the neural circuits responsible for implementation, encoding, and updating of rules[3].

AUTHOR CONTRIBUTIONS

Conceptualization, Y.-T.C., E.A.F. and D.H.O.; Investigation, Y.-T.C.; Methodology, Y.-T.C., E.A.F. and D.X.; Formal Analysis, Y.-T.C.; Writing – Original Draft, Y.-T.C. and D.H.O.; Writing – Review & Editing, Y.-T.C. and D.H.O.; Funding Acquisition, D.H.O.; Resources, D.H.O.; Supervision, D.H.O.

ACKNOWLEDGEMENTS

We thank William Olson for comments on the manuscript; Emily Lubin and Jae Hun Lee for technical assistance; and Genki Minamisawa for technical advice. This work was supported by a Government Scholarship to Study Abroad from the Ministry of Education of Taiwan to Y.-T. C., Seed Grant S-2021-GR-045 from The Kavli Foundation to D.H.O., and NIH grants R01NS089652 and 1R01NS104834-01 to D.H.O.

REFERENCES

1. Miller, E.K., and Cohen, J.D. (2001). An Integrative Theory of Prefrontal Cortex Function.

Annu. Rev. Neurosci. *24*, 167–202. 10.1146/annurev.neuro.24.1.167.
2. Koechlin, E. (2014). An evolutionary computational theory of prefrontal executive function in decision-making. Philos. Trans. R. Soc. B Biol. Sci. *369*, 20130474. 10.1098/rstb.2013.0474.
3. Mansouri, F.A., Freedman, D.J., and Buckley, M.J. (2020). Emergence of abstract rules in the primate brain. Nat. Rev. Neurosci. *21*, 595–610. 10.1038/s41583-020-0364-5.
4. Gastgeb, H.Z., Dundas, E.M., Minshew, N.J., and Strauss, M.S. (2012). Category formation in autism: can individuals with autism form categories and prototypes of dot patterns? J. Autism Dev. Disord. *42*, 1694–1704. 10.1007/s10803-011-1411-x.
5. Jones, E.J.H., Webb, S.J., Estes, A., and Dawson, G. (2013). Rule learning in autism: the role of reward type and social context. Dev. Neuropsychol. *38*, 58–77. 10.1080/87565641.2012.727049.
6. Weinberger, D.R., and Berman, K.F. (1996). Prefrontal function in schizophrenia: confounds and controversies. Philos. Trans. R. Soc. Lond. B. Biol. Sci. *351*, 1495–1503. 10.1098/rstb.1996.0135.
7. Woodward, N.D., Karbasforoushan, H., and Heckers, S. (2012). Thalamocortical dysconnectivity in schizophrenia. Am. J. Psychiatry *169*, 1092–1099. 10.1176/appi.ajp.2012.12010056.
8. Bari, B.A., Grossman, C.D., Lubin, E.E., Rajagopalan, A.E., Cressy, J.I., and Cohen, J.Y. (2019). Stable Representations of Decision Variables for Flexible Behavior. Neuron *103*, 922-933.e7. 10.1016/j.neuron.2019.06.001.
9. Hattori, R., and Komiyama, T. (2021). Context-dependent persistency as a coding mechanism for robust and widely distributed value coding. Neuron, S0896-6273(21)00891-6. 10.1016/j.neuron.2021.11.001.
10. Kamigaki, T., Fukushima, T., and Miyashita, Y. (2009). Cognitive Set Reconfiguration Signaled by Macaque Posterior Parietal Neurons. Neuron *61*, 941–951. 10.1016/j.neuron.2009.01.028.
11. Rodgers, C.C., and DeWeese, M.R. (2014). Neural Correlates of Task Switching in Prefrontal Cortex and Primary Auditory Cortex in a Novel Stimulus Selection Task for Rodents. Neuron *82*, 1157–1170. 10.1016/j.neuron.2014.04.031.
12. Sakai, K. (2008). Task Set and Prefrontal Cortex. Annu. Rev. Neurosci. *31*, 219–245. 10.1146/annurev.neuro.31.060407.125642.
13. van den Brink, R.L., Hagena, K., Wilming, N., Murphy, P.R., Büchel, C., and Donner, T.H. (2023). Flexible sensory-motor mapping rules manifest in correlated variability of stimulus and action codes across the brain. Neuron *111*, 571-584.e9. 10.1016/j.neuron.2022.11.009.
14. Crochet, S., Lee, S.-H., and Petersen, C.C.H. (2019). Neural Circuits for Goal-Directed Sensorimotor Transformations. Trends Neurosci. *42*, 66–77. 10.1016/j.tins.2018.08.011.
15. Esmaeili, V., Tamura, K., Muscinelli, S.P., Modirshanechi, A., Boscaglia, M., Lee, A.B., Oryshchuk, A., Foustoukos, G., Liu, Y., Crochet, S., et al. (2021). Rapid suppression and sustained activation of distinct cortical regions for a delayed sensory-triggered motor response. Neuron *109*, 2183-2201.e9. 10.1016/j.neuron.2021.05.005.
16. Petersen, C.C.H. (2019). Sensorimotor processing in the rodent barrel cortex. Nat. Rev. Neurosci. *20*, 533–546. 10.1038/s41583-019-0200-y.
17. Svoboda, K., and Li, N. (2018). Neural mechanisms of movement planning: motor cortex and beyond. Curr. Opin. Neurobiol. *49*, 33–41. 10.1016/j.conb.2017.10.023.
18. Guo, Z.V., Li, N., Huber, D., Ophir, E., Gutnisky, D., Ting, J.T., Feng, G., and Svoboda, K. (2014). Flow of Cortical Activity Underlying a Tactile Decision in Mice. Neuron *81*, 179–194. 10.1016/j.neuron.2013.10.020.
19. Mao, T., Kusefoglu, D., Hooks, B.M., Huber, D., Petreanu, L., and Svoboda, K. (2011). Long-range neuronal circuits underlying the interaction between sensory and motor cortex. Neuron *72*, 111–123. 10.1016/j.neuron.2011.07.029.

20. Matyas, F., Sreenivasan, V., Marbach, F., Wacongne, C., Barsy, B., Mateo, C., Aronoff, R., and Petersen, C.C.H. (2010). Motor Control by Sensory Cortex. Science *330*, 1240–1243. 10.1126/science.1195797.
21. Chen, T.-W., Li, N., Daie, K., and Svoboda, K. (2017). A Map of Anticipatory Activity in Mouse Motor Cortex. Neuron *94*, 866-879.e4. 10.1016/j.neuron.2017.05.005.
22. Condylis, C., Lowet, E., Ni, J., Bistrong, K., Ouellette, T., Josephs, N., and Chen, J.L. (2020). Context-Dependent Sensory Processing across Primary and Secondary Somatosensory Cortex. Neuron *106*, 515-525.e5. 10.1016/j.neuron.2020.02.004.
23. Steinmetz, N.A., Zatka-Haas, P., Carandini, M., and Harris, K.D. (2019). Distributed coding of choice, action and engagement across the mouse brain. Nature *576*, 266–273. 10.1038/s41586-019-1787-x.
24. Zhang, S., Xu, M., Kamigaki, T., Hoang Do, J.P., Chang, W.-C., Jenvay, S., Miyamichi, K., Luo, L., and Dan, Y. (2014). Long-range and local circuits for top-down modulation of visual cortex processing. Science *345*, 660–665. 10.1126/science.1254126.
25. Afshar, A., Santhanam, G., Yu, B.M., Ryu, S.I., Sahani, M., and Shenoy, K.V. (2011). Single-trial neural correlates of arm movement preparation. Neuron *71*, 555–564. 10.1016/j.neuron.2011.05.047.
26. Churchland, M.M., Santhanam, G., and Shenoy, K.V. (2006). Preparatory activity in premotor and motor cortex reflects the speed of the upcoming reach. J. Neurophysiol. *96*, 3130–3146. 10.1152/jn.00307.2006.
27. Churchland, M.M., Cunningham, J.P., Kaufman, M.T., Foster, J.D., Nuyujukian, P., Ryu, S.I., and Shenoy, K.V. (2012). Neural population dynamics during reaching. Nature *487*, 51–56. 10.1038/nature11129.
28. Sauerbrei, B.A., Guo, J.-Z., Cohen, J.D., Mischiati, M., Guo, W., Kabra, M., Verma, N., Mensh, B., Branson, K., and Hantman, A.W. (2020). Cortical pattern generation during dexterous movement is input-driven. Nature *577*, 386–391. 10.1038/s41586-019-1869-9.
29. Buonomano, D.V., and Maass, W. (2009). State-dependent computations: spatiotemporal processing in cortical networks. Nat. Rev. Neurosci. *10*, 113–125. 10.1038/nrn2558.
30. Remington, E.D., Narain, D., Hosseini, E.A., and Jazayeri, M. (2018). Flexible Sensorimotor Computations through Rapid Reconfiguration of Cortical Dynamics. Neuron *98*, 1005-1019.e5. 10.1016/j.neuron.2018.05.020.
31. Wang, J., Narain, D., Hosseini, E.A., and Jazayeri, M. (2018). Flexible timing by temporal scaling of cortical responses. Nat. Neurosci. *21*, 102–110. 10.1038/s41593-017-0028-6.
32. Finkelstein, A., Fontolan, L., Economo, M.N., Li, N., Romani, S., and Svoboda, K. (2021). Attractor dynamics gate cortical information flow during decision-making. Nat. Neurosci. *24*, 843–850. 10.1038/s41593-021-00840-6.
33. Gao, Z., Davis, C., Thomas, A.M., Economo, M.N., Abrego, A.M., Svoboda, K., De Zeeuw, C.I., and Li, N. (2018). A cortico-cerebellar loop for motor planning. Nature *563*, 113–116. 10.1038/s41586-018-0633-x.
34. Mante, V., Sussillo, D., Shenoy, K.V., and Newsome, W.T. (2013). Context-dependent computation by recurrent dynamics in prefrontal cortex. Nature *503*, 78–84. 10.1038/nature12742.
35. Raposo, D., Kaufman, M.T., and Churchland, A.K. (2014). A category-free neural population supports evolving demands during decision-making. Nat. Neurosci. *17*, 1784–1792. 10.1038/nn.3865.
36. Vyas, S., Golub, M.D., Sussillo, D., and Shenoy, K.V. (2020). Computation Through Neural Population Dynamics. Annu. Rev. Neurosci. *43*, 249–275. 10.1146/annurev-neuro-092619-094115.
37. Churchland, M.M., Cunningham, J.P., Kaufman, M.T., Ryu, S.I., and Shenoy, K.V. (2010). Cortical Preparatory Activity: Representation of Movement or First Cog in a Dynamical Machine? Neuron *68*, 387–400. 10.1016/j.neuron.2010.09.015.

38. Shenoy, K.V., Sahani, M., and Churchland, M.M. (2013). Cortical Control of Arm Movements: A Dynamical Systems Perspective. Annu. Rev. Neurosci. *36*, 337–359. 10.1146/annurev-neuro-062111-150509.
39. Chevée, M., Finkel, E.A., Kim, S.-J., O'Connor, D.H., and Brown, S.P. (2021). Neural activity in the mouse claustrum in a cross-modal sensory selection task. Neuron, S089662732100951X. 10.1016/j.neuron.2021.11.013.
40. Ebitz, R.B., and Hayden, B.Y. (2021). The population doctrine in cognitive neuroscience. Neuron *109*, 3055–3068. 10.1016/j.neuron.2021.07.011.
41. Foffani, G., and Moxon, K.A. (2004). PSTH-based classification of sensory stimuli using ensembles of single neurons. J. Neurosci. Methods *135*, 107–120. 10.1016/j.jneumeth.2003.12.011.
42. O'Connor, D.H., Peron, S.P., Huber, D., and Svoboda, K. (2010). Neural activity in barrel cortex underlying vibrissa-based object localization in mice. Neuron *67*, 1048–1061. 10.1016/j.neuron.2010.08.026.
43. Cunningham, J.P., and Yu, B.M. (2014). Dimensionality reduction for large-scale neural recordings. Nat. Neurosci. *17*, 1500–1509. 10.1038/nn.3776.
44. Elsayed, G.F., Lara, A.H., Kaufman, M.T., Churchland, M.M., and Cunningham, J.P. (2016). Reorganization between preparatory and movement population responses in motor cortex. Nat. Commun. *7*, 13239. 10.1038/ncomms13239.
45. Russo, A.A., Khajeh, R., Bittner, S.R., Perkins, S.M., Cunningham, J.P., Abbott, L.F., and Churchland, M.M. (2020). Neural Trajectories in the Supplementary Motor Area and Motor Cortex Exhibit Distinct Geometries, Compatible with Different Classes of Computation. Neuron *107*, 745-758.e6. 10.1016/j.neuron.2020.05.020.
46. Ruff, D.A., and Cohen, M.R. (2019). Simultaneous multi-area recordings suggest that attention improves performance by reshaping stimulus representations. Nat. Neurosci. *22*, 1669–1676. 10.1038/s41593-019-0477-1.
47. Li, N., Daie, K., Svoboda, K., and Druckmann, S. (2016). Robust neuronal dynamics in premotor cortex during motor planning. Nature *532*, 459–464. 10.1038/nature17643.
48. Yang, W., Tipparaju, S.L., Chen, G., and Li, N. (2022). Thalamus-driven functional populations in frontal cortex support decision-making. Nat. Neurosci. *25*, 1339–1352. 10.1038/s41593-022-01171-w.
49. Sachidhanandam, S., Sreenivasan, V., Kyriakatos, A., Kremer, Y., and Petersen, C.C.H. (2013). Membrane potential correlates of sensory perception in mouse barrel cortex. Nat. Neurosci. *16*, 1671–1677. 10.1038/nn.3532.
50. Le Merre, P., Esmaeili, V., Charrière, E., Galan, K., Salin, P.-A., Petersen, C.C.H., and Crochet, S. (2018). Reward-Based Learning Drives Rapid Sensory Signals in Medial Prefrontal Cortex and Dorsal Hippocampus Necessary for Goal-Directed Behavior. Neuron *97*, 83-91.e5. 10.1016/j.neuron.2017.11.031.
51. Mohan, H., Gallero-Salas, Y., Carta, S., Sacramento, J., Laurenczy, B., Sumanovski, L.T., de Kock, C.P.J., Helmchen, F., and Sachidhanandam, S. (2018). Sensory representation of an auditory cued tactile stimulus in the posterior parietal cortex of the mouse. Sci. Rep. *8*, 7739. 10.1038/s41598-018-25891-x.
52. Olcese, U., Iurilli, G., and Medini, P. (2013). Cellular and synaptic architecture of multisensory integration in the mouse neocortex. Neuron *79*, 579–593. 10.1016/j.neuron.2013.06.010.
53. Song, Y.-H., Kim, J.-H., Jeong, H.-W., Choi, I., Jeong, D., Kim, K., and Lee, S.-H. (2017). A Neural Circuit for Auditory Dominance over Visual Perception. Neuron *93*, 940-954.e6. 10.1016/j.neuron.2017.01.006.
54. Funamizu, A., Kuhn, B., and Doya, K. (2016). Neural substrate of dynamic Bayesian inference in the cerebral cortex. Nat. Neurosci. *19*, 1682–1689. 10.1038/nn.4390.
55. Gallero-Salas, Y., Han, S., Sych, Y., Voigt, F.F., Laurenczy, B., Gilad, A., and Helmchen, F.

(2021). Sensory and Behavioral Components of Neocortical Signal Flow in Discrimination Tasks with Short-Term Memory. Neuron *109*, 135-148.e6. 10.1016/j.neuron.2020.10.017.
56. Goard, M.J., Pho, G.N., Woodson, J., and Sur, M. (2016). Distinct roles of visual, parietal, and frontal motor cortices in memory-guided sensorimotor decisions. eLife *5*, e13764. 10.7554/eLife.13764.
57. Harvey, C.D., Coen, P., and Tank, D.W. (2012). Choice-specific sequences in parietal cortex during a virtual-navigation decision task. Nature *484*, 62–68. 10.1038/nature10918.
58. Mohan, H., de Haan, R., Broersen, R., Pieneman, A.W., Helmchen, F., Staiger, J.F., Mansvelder, H.D., and de Kock, C.P.J. (2019). Functional Architecture and Encoding of Tactile Sensorimotor Behavior in Rat Posterior Parietal Cortex. J. Neurosci. Off. J. Soc. Neurosci. *39*, 7332–7343. 10.1523/JNEUROSCI.0693-19.2019.
59. Chubykin, A.A., Roach, E.B., Bear, M.F., and Shuler, M.G.H. (2013). A Cholinergic Mechanism for Reward Timing within Primary Visual Cortex. Neuron *77*, 723–735. 10.1016/j.neuron.2012.12.039.
60. Lacefield, C.O., Pnevmatikakis, E.A., Paninski, L., and Bruno, R.M. (2019). Reinforcement Learning Recruits Somata and Apical Dendrites across Layers of Primary Sensory Cortex. Cell Rep. *26*, 2000-2008.e2. 10.1016/j.celrep.2019.01.093.
61. Musall, S., Kaufman, M.T., Juavinett, A.L., Gluf, S., and Churchland, A.K. (2019). Single-trial neural dynamics are dominated by richly varied movements. Nat. Neurosci. *22*, 1677–1686. 10.1038/s41593-019-0502-4.
62. Shuler, M.G., and Bear, M.F. (2006). Reward Timing in the Primary Visual Cortex. Science *311*, 1606–1609. 10.1126/science.1123513.
63. Moore, T., and Zirnsak, M. (2017). Neural Mechanisms of Selective Visual Attention. Annu. Rev. Psychol. *68*, 47–72. 10.1146/annurev-psych-122414-033400.
64. Rizzolatti, G., Riggio, L., Dascola, I., and Umiltá, C. (1987). Reorienting attention across the horizontal and vertical meridians: evidence in favor of a premotor theory of attention. Neuropsychologia *25*, 31–40. 10.1016/0028-3932(87)90041-8.
65. Moore, T., and Armstrong, K.M. (2003). Selective gating of visual signals by microstimulation of frontal cortex. Nature *421*, 370–373. 10.1038/nature01341.
66. Moore, T., and Fallah, M. (2001). Control of eye movements and spatial attention. Proc. Natl. Acad. Sci. *98*, 1273–1276. 10.1073/pnas.98.3.1273.
67. Aruljothi, K., Marrero, K., Zhang, Z., Zareian, B., and Zagha, E. (2020). Functional Localization of an Attenuating Filter within Cortex for a Selective Detection Task in Mice. J. Neurosci. Off. J. Soc. Neurosci. *40*, 5443–5454. 10.1523/JNEUROSCI.2993-19.2020.
68. Borden, P.Y., Wright, N.C., Morrissette, A.E., Jaeger, D., Haider, B., and Stanley, G.B. (2022). Thalamic bursting and the role of timing and synchrony in thalamocortical signaling in the awake mouse. Neuron *110*, 2836-2853.e8. 10.1016/j.neuron.2022.06.008.
69. Zhang, Z., and Zagha, E. (2022). Frontal Cortex Gates Distractor Stimulus Encoding in Sensory Cortex (Neuroscience) 10.1101/2022.03.31.486430.
70. Zhang, S., Xu, M., Chang, W.-C., Ma, C., Hoang Do, J.P., Jeong, D., Lei, T., Fan, J.L., and Dan, Y. (2016). Organization of long-range inputs and outputs of frontal cortex for top-down control. Nat. Neurosci. *19*, 1733–1742. 10.1038/nn.4417.
71. Churchland, M.M. (2006). Neural Variability in Premotor Cortex Provides a Signature of Motor Preparation. J. Neurosci. *26*, 3697–3712. 10.1523/JNEUROSCI.3762-05.2006.
72. Jonikaitis, D., Nissim, N., Xia, R., and Moore, T. (2020). Robust Encoding of Abstract Rules by Distinct Neuronal Populations in Primate Visual Cortex. bioRxiv, 2020.10.28.351460. 10.1101/2020.10.28.351460.
73. Guo, Z.V., Inagaki, H.K., Daie, K., Druckmann, S., Gerfen, C.R., and Svoboda, K. (2017). Maintenance of persistent activity in a frontal thalamocortical loop. Nature *545*, 181–186. 10.1038/nature22324.
74. Oude Lohuis, M.N., Pie, J.L., Marchesi, P., Montijn, J.S., de Kock, C.P.J., Pennartz, C.M.A.,

and Olcese, U. (2022). Multisensory task demands temporally extend the causal requirement for visual cortex in perception. Nat. Commun. *13*, 2864. 10.1038/s41467-022-30600-4.
75. Siniscalchi, M.J., Phoumthipphavong, V., Ali, F., Lozano, M., and Kwan, A.C. (2016). Fast and slow transitions in frontal ensemble activity during flexible sensorimotor behavior. Nat. Neurosci. *19*, 1234–1242. 10.1038/nn.4342.
76. Buffalo, E.A., Fries, P., Landman, R., Liang, H., and Desimone, R. (2010). A backward progression of attentional effects in the ventral stream. Proc. Natl. Acad. Sci. U. S. A. *107*, 361–365. 10.1073/pnas.0907658106.
77. Gregoriou, G.G., Gotts, S.J., Zhou, H., and Desimone, R. (2009). High-Frequency, Long-Range Coupling Between Prefrontal and Visual Cortex During Attention. Science *324*, 1207–1210. 10.1126/science.1171402.
78. Hsiao, S.S., O'Shaughnessy, D.M., and Johnson, K.O. (1993). Effects of selective attention on spatial form processing in monkey primary and secondary somatosensory cortex. J. Neurophysiol. *70*, 444–447. 10.1152/jn.1993.70.1.444.
79. Lee, S., Carvell, G.E., and Simons, D.J. (2008). Motor modulation of afferent somatosensory circuits. Nat. Neurosci. *11*, 1430–1438. 10.1038/nn.2227.
80. Zagha, E., Casale, A.E., Sachdev, R.N.S., McGinley, M.J., and McCormick, D.A. (2013). Motor Cortex Feedback Influences Sensory Processing by Modulating Network State. Neuron *79*, 567–578. 10.1016/j.neuron.2013.06.008.
81. Anastasiades, P.G., and Carter, A.G. (2021). Circuit organization of the rodent medial prefrontal cortex. Trends Neurosci. *44*, 550–563. 10.1016/j.tins.2021.03.006.
82. Schmitt, L.I., Wimmer, R.D., Nakajima, M., Happ, M., Mofakham, S., and Halassa, M.M. (2017). Thalamic amplification of cortical connectivity sustains attentional control. Nature *545*, 219–223. 10.1038/nature22073.
83. Hippenmeyer, S., Vrieseling, E., Sigrist, M., Portmann, T., Laengle, C., Ladle, D.R., and Arber, S. (2005). A Developmental Switch in the Response of DRG Neurons to ETS Transcription Factor Signaling. PLoS Biol. *3*, e159. 10.1371/journal.pbio.0030159.
84. Madisen, L., Mao, T., Koch, H., Zhuo, J., Berenyi, A., Fujisawa, S., Hsu, Y.-W.A., Garcia, A.J., Gu, X., Zanella, S., et al. (2012). A toolbox of Cre-dependent optogenetic transgenic mice for light-induced activation and silencing. Nat. Neurosci. *15*, 793–802. 10.1038/nn.3078.
85. Gorski, J.A., Talley, T., Qiu, M., Puelles, L., Rubenstein, J.L.R., and Jones, K.R. (2002). Cortical Excitatory Neurons and Glia, But Not GABAergic Neurons, Are Produced in the Emx1-Expressing Lineage. J. Neurosci. *22*, 6309–6314. 10.1523/JNEUROSCI.22-15-06309.2002.
86. Zhao, S., Ting, J.T., Atallah, H.E., Qiu, L., Tan, J., Gloss, B., Augustine, G.J., Deisseroth, K., Luo, M., Graybiel, A.M., et al. (2011). Cell type–specific channelrhodopsin-2 transgenic mice for optogenetic dissection of neural circuitry function. Nat. Methods *8*, 745–752. 10.1038/nmeth.1668.
87. Masino, S.A., Kwon, M.C., Dory, Y., and Frostig, R.D. (1993). Characterization of functional organization within rat barrel cortex using intrinsic signal optical imaging through a thinned skull. Proc. Natl. Acad. Sci. U. S. A. *90*, 9998–10002. 10.1073/pnas.90.21.9998.
88. O'Connor, D.H., Hires, S.A., Guo, Z.V., Li, N., Yu, J., Sun, Q.-Q., Huber, D., and Svoboda, K. (2013). Neural coding during active somatosensation revealed using illusory touch. Nat. Neurosci. *16*, 958–965. 10.1038/nn.3419.
89. Pachitariu, M., Steinmetz, N., Kadir, S., Carandini, M., and Kenneth D., H. (2016). Kilosort: realtime spike-sorting for extracellular electrophysiology with hundreds of channels (Neuroscience) 10.1101/061481.
90. Saravanan, V., Berman, G.J., and Sober, S.J. (2019). Application of the Hierarchical Bootstrap to Multi-Level Data in Neuroscience (Neuroscience) 10.1101/819334.

METHODS

Mice

All procedures were performed in accordance with protocols approved by the Johns Hopkins University Animal Care and Use Committee. Twelve mice (8 male, 4 female) were obtained by crossing *PV*^{cre} lines[83] (Jackson Labs: 008069) with Ai32 lines[84] (Jackson Labs: 012569). Seven *PV*^{cre}; Ai32 mice (5 male, 2 female) were trained to perform the cross-modal selection task and included in behavioral and optogenetic inhibition experiments. Five *PV*^{cre}; Ai32 mice (3 male, 2 female) were trained to perform the tactile detection task and included in optogenetic inhibition experiments. Four male mice included in behavioral experiments were obtained by crossing *Emx1*^{cre} mice[85] (Jackson Labs: 005628) with Ai32 mice. Two male mice included in behavioral experiments were heterozygous *VGAT*$^{ChR2\text{-}EYFP}$ (Jackson Labs: 014548)[86]. Mice ranged in age from 2-5 months at the start of training. Mice were housed in a vivarium with a reverse light-dark cycle (12 h each phase), and were singly housed after surgery and during behavioral experiments. Details of assignment to different experimental conditions are listed in Table 1.

Behavioral task

All behavioral experiments were conducted with head-fixed mice during the dark phase. Behavioral apparatus was controlled by BControl software (C. Brody, Princeton University). Four to 7 days after a headpost implantation and 7-14 days before behavioral training, mice were allowed 1 mL of water daily until reaching ~80% of their starting body weight. On training days, mice were allowed to perform until sated (~ 1 hr/ day) and were weighed before and after each session to determine the amount of water consumed. Additional water was given if mice consumed <0.3 mL of water in order to maintain a stable body weight. On days when their behavior was not tested, they received 1 mL of water.

Cross-modal sensory selection task

The cross-modal sensory selection training consists of two stages. Mice were first trained to perform tactile and visual detection separately, then trained on the cross-modal selection task where tactile and visual stimuli were randomly interleaved.

In the first 1-2 sessions, mice were acclimated to head fixation in the behavioral apparatus while being given free access to water via two reward ports located 6-10 mm and ~35 degrees to the left and right of the mouse midline. In subsequent sessions, mice were randomly assigned to start with tactile or visual detection training. After the hit rate of one modality reached >70% (~3 days; hit rate = 100*(# hits) / (# hits + # misses)), stimulus detection training of the other modality began. For tactile detection training, a single whisker (always on the right whisker pad) was threaded into a glass pipette attached to a piezo actuator (D220-A4-203YB, Piezo Systems), which was driven by a piezo controller (MDTC93B, Thorlabs). Approximately 1.5 mm of whisker remained exposed at the base. All whiskers except the target whisker were trimmed to near the base. Mice were given a drop of water (~6 µl) for licking to the right reward port in response to a tactile stimulus (1 s sinusoidal deflections at 40 Hz, ~1400 deg / s) during an answer period (0.1 to 2 s from stimulus onset). For visual detection training, mice were rewarded for licking to the left water port in response to a visual stimulus. Each visual stimulus comprised 470 nm light (1 s flash at ~5 mW) generated by an LED (M470F1 LED driven by

LEDD1B, Thorlabs) and emitted from the tip of an optic fiber (105 μm diameter, 0.22 NA; M43L01, Thorlabs) positioned 5.5 cm away from the tip of the mouse's nose along its midline. To reduce compulsive licking, licks that occurred within a "grace period" (0 to 0.1 s from stimulus onset) were not rewarded. Licks occurring in a "censor period" (-0.2 to 0 s from stimulus onset) resulted in the withholding of the stimulus presentation for that trial and no reward or punishment. Trials with licks occurring in the grace and censor periods were omitted from analysis. In all sessions, ambient white noise (cut off at 40 kHz, ~80 dB SPL) was played to mask any potential sound associated with movement of the piezo stimulator.

After the stimulus-detection training, mice were trained to perform the cross-modal selection task. Tactile and visual stimuli were randomly interleaved (subject to a limit of 4 consecutive trials of the same type) and trials were separated by a random interval (3.5 s fixed interval + random interval drawn from an exponential distribution with mean 4 s). Trials were grouped into either respond-to-touch or respond-to-light blocks (54-66 trials per block from an uniform distribution with mean 60 trials). Each session randomly began with one of two block types, and the block types subsequently alternated multiple times (4-6 blocks per session). In respond-to-touch blocks, mice were rewarded with a drop of water if they licked the right reward port following tactile but not visual stimuli. In respond-to-light blocks, mice were rewarded with a drop of water for licking the left reward port following visual but not tactile stimuli. The answer, grace and censor periods were as described above for the stimulus-detection training.

Four trial outcomes were defined based on block types, sensory stimuli, and responses (Fig. 1c). Trials in which mice licked to the correct reward port following tactile stimuli in respond-to-touch blocks or visual stimuli in respond-to-light blocks were scored as "hit" trials. Failures to lick to the correct port after tactile stimuli in respond-to-touch blocks or visual stimuli in respond-to-light blocks were scored as "miss" trials. Licks to either reward port after tactile stimuli in respond-to-light blocks, visual stimuli in respond-to-touch blocks, or to the incorrect reward port after either stimulus type, resulted in "false alarm" trials. Trials in which mice correctly withheld licks after tactile stimuli in respond-to-light blocks, or after visual stimuli in respond-to-touch blocks, were scored as "correct rejection" trials. Performance was quantified as percent correct: 100*(# hits + # correct rejections) / (# of trials total).

In an initial stage of cross-modal selection training (~7 sessions), a drop of water from the rewarded port was automatically released following 80% behaviorally relevant stimuli. Subsequently, automatically released water only occurred on the 9th trial after a block switch. Once performance reached >70% of trials correct, task difficulty was gradually increased by reducing stimulus intensity and duration. In a final stage of training, faint stimuli (tactile: 0.15 s sinusoidal deflections at 20 Hz, ~800 deg/s; visual: 0.15 s flash at ~3 μW) were used to increase cognitive load and to result in error trials for analysis. Mice were considered trained when performance reached >70% correct for at least three consecutive days. After reaching this performance criterion, mice proceeded with test sessions. Seven *PV*^{cre}; Ai32 mice performed the cross-modal task during inhibition experiments, and six of them continued for electrophysiology recordings. Other transgenic mice were given test sessions for electrophysiology recordings but not optogenetic experiments.

Behavioral sessions lasted until mice were sated. To ensure stable engagement, the last 20 trials of each session were removed from further analysis. In addition, sessions were omitted

from analysis if overall performance was < 60% correct, at least one of block performances (respond-to-touch or respond-to-light blocks) was < 55% correct, or at least one of hit rates (tactile or visual hits) was < 35%. Three sessions in total were removed for these reasons (from two mice).

Tactile detection task

Head-fixed mice were trained to perform a go/no-go tactile detection task. On Go trials, the whisker was deflected (0.15 s sinusoidal deflections at 20 Hz, ~600 deg/s). If mice licked the right reward port following a tactile stimulus, a drop of water was released and it was scored as a hit trial. If mice failed to respond to a tactile stimulus, it was scored as a miss trial. On NoGo trials, the target whisker was not deflected. If mice licked during the answer period, it was scored as a false alarm. If mice withheld licking, it was scored as a correct rejection. Go and NoGo trials were randomly interleaved (subject to a limit of 4 consecutive trials of the same type), and no trial-start cue was presented. The answer, grace and censor periods were as described above for the cross-modal selection task. Tactile stimuli of the tactile detection task were slightly weaker compared with the cross-modal selection task in order to control task difficulties by making behavioral performance similar (~75% correct).

Similar to the cross-modal selection task, the last 20 trials in each session were excluded, and sessions with performance < 60% correct or tactile hit rate < 35% were removed from subsequent analysis. Five *PV*^{cre}; Ai32 mice performed the tactile detection task during inhibition experiments.

Surgery

Prior to behavioral testing, mice were implanted with clear-skull caps[18] and metal headposts designed to expose a large area of the dorsal surface of the skull. During surgery, mice were anesthetized under isoflurane (1-2% in O2; Surgivet) and mounted in a stereotaxic apparatus (David Kopf Instruments) with a thermal blanket (Harvard Apparatus). Mice were given a subcutaneous injection of Marcaine or Lidocaine for local analgesia and an intraperitoneal injection of Ketoprofen to reduce inflammation. The scalp and periosteum over the dorsal surface of the skull were removed. To expose S2 on the left hemisphere, the left temporal muscle was detached and the bone ridge at the temporal-parietal junction was thinned using a dental drill. Headposts were fixed to the skull over the lambda structure using clear adhesive luting cement (C&B Metabond Quick Adhesive Cement System; Parkell). A thin layer of clear cement followed by an additional layer of cyanoacrylate glue (Krazy Glue) was applied to the entire surface of the exposed skull, leaving it largely transparent. To protect the clear skull from scratching, a silicone elastomer (Kwik-Cats) was applied prior to optogenetic experiments.

Intrinsic signal imaging (ISI) was used to guide the whisker parts of S1 and S2 for neural recordings and optogenetic experiments[87,88]. Mice were lightly anesthetized with isoflurane (0.5-1%) and chlorprothixene. The C2 or C3 whisker was stimulated with a Piezo at 10 Hz. Since S2 is close to the auditory cortex, white noise was played during imaging.

For silicon probe recording, a small craniotomy (~1 mm in diameter) over the recording site (always on the left hemisphere) was made (S1 and S2 determined by ISI; MM: 1.5 mm anterior,

1.0 mm lateral; ALM: 2.5 mm anterior, 1.5 mm lateral to bregma). The dental acrylic and skull was thinned using a dental drill and the remaining bone was removed with a tungsten needle or forceps. A separate, smaller craniotomy (~0.6 mm in diameter) on the right hemisphere was made for implantation of a ground screw (0.6 mm anterior, 3.0 mm lateral to bregma; S1 trunk region). Additional craniotomies were usually made in new locations after finishing recordings in previous ones (12 mice; 1-4 recording sites per mouse).

Electrophysiology and data preprocessing

Linear 64-channel probes (H3, Cambridge NeuroTech) were coated with DiI (saturated) or DiD (5-10mg/mL) to histologically verify the site of recording post hoc. The silicon probe was inserted into the cortex either vertically (for MM and ALM) or at ~ 40 degrees from vertical (for S1 and S2). After probe insertion, the brain was covered with a layer of 1.5% agarose and ACSF and was left for ~10 minutes prior to recording.

Neural signals and behavioral timestamps were recorded using an Intan system (RHD2000 series multi-channel amplifier chip; Intan Technologies). Neural signals were sampled at 30 kHz. Kilosort was used for spike sorting[89] and spike clusters were manually curated using Phy. Units were excluded from further analysis if the rate of inter-spike-interval violations within a 1.5 ms window was >0.5%, L-ratios were >0.1, the presence of spikes was <90% of the whole session, the cumulative drift of spike depth was >40 um (Unit Quality Metrics, Allen Institute).

For analyses about stimulus-evoked responses, neural spike rates were calculated in10 ms bins and smoothed with a Gaussian kernel (50 ms). For analyses about pre-stimulus activity, neural spike rates were calculated in 100 ms bins without smoothing. Spike rates of simultaneously recorded neurons were normalized for all population-level analyses including linear discriminant analysis and principal component analysis. We used soft normalization to make activity in a roughly unity range and to reduce the impact of units with low firing rate (normalized response = (response-mean(response))/(range(response)+5))[27,45]. In addition, to minimize movement effects on neural activity during the pre-stimulus window (-1 to 0 s from stimulus onset), trials with licking occurring in this window were removed (~25%).

Optogenetic inhibition

PV^{cre}; Ai32 mice implanted with clear-skull caps were given optogenetic inhibition experiments after behavioral task training (cross-modal selection or tactile detection). Laser stimuli (473 nm; MBL-III-473-100, Ultralasers) were directed to the brain via optic fibers (200 µm diameter, 0.22 NA; TM200FL1B, Thorlabs) positioned over (~2 mm above) the cortical areas bilaterally (8-10 mW each side). For S1 and S2, the left whisker areas were guided by intrinsic signal imaging (as described above) and the right whisker areas were determined as the symmetric positions. Other targeted areas on the dorsal cortex included MM (1.5 mm anterior, 1.0 mm lateral to bregma), ALM (2.5 mm anterior, 1.5 mm lateral), AMM (2.5 mm anterior, 0.5 mm lateral), and PPC (1.94 mm posterior, 1.6 mm lateral). Sham sessions were identical to optogenetic inhibition sessions except that the dorsal cortex was covered by blackout cloth in order to not inhibit any brain areas. For each session, one of the cortical areas or the sham condition was randomly assigned for inhibition. A cone, blackout cloth and tape were used to shield the mouse's eyes from scattered light due to the laser.

For the cross-modal sensory selection task, laser stimuli were delivered to the targeted brain areas in ~30% of tactile and visual stimulus trials. In around half of these trials, optogenetic inhibition occurred before stimulus onset to suppress baseline activity (-0.8 to 0 s from stimulus onset, 40 Hz sinusoidal waveform with a 0.1 s linearly modulated ramp-down at the end). In the other half of these trials, optogenetic inhibition began simultaneously with the stimulus onset to suppress sensory-evoked activity (0 to 2 s from stimulus onset, 40 Hz sinusoidal waveform with a 0.2 s linearly modulated ramp-down at the end). Additionally, in a subset of trials (~20%), laser stimuli were delivered alone. These “laser only” trials consisted of short (0.8 s) and long (2 s) trains of laser pulses that are identical to the laser stimuli in pre-stimulus-onset and post-stimulus-onset conditions respectively.

For the tactile detection task, laser stimuli were delivered in ~30% of trials. Among these laser trials, Go trials consist of approximately half and half pre-stimulus-onset and post-stimulus-onset inhibition. Since there was no tactile stimulus in NoGo trials, short (0.8 s) and long (2 s) laser stimuli were delivered before and after trial onset respectively. Laser stimuli are identical to those used in the cross-modal selection task.

Baseline behavioral performance was measured by trials without laser stimuli and used to determine if a session passed the criteria of good performance (as described in the behavioral task section). In addition, sessions with laser catch rates >75% or > hit rates were removed from analysis because a high laser catch rate indicates that mice detected laser stimuli instead of tactile or visual stimuli (laser catch rate = 100*(# of laser only trials in which licking occurred) / (# of laser only trials total)).

Single-neuron discrimination analyses

Receiver-Operating Characteristic (ROC) analysis

ROC analysis was used to calculate how well trial-by-trial activity of a single neuron could discriminate certain conditions (e.g., tactile hit vs tactile correct rejection). The area under the ROC curve (AUC) represents the performance of an ideal observer in discriminating trials based on these conditions (MATLAB “perfcurve”). For discriminability of touch-evoked activity between task rules (Fig. 1h), tactile correct trials were split into tactile hits (respond-to-touch) and tactile correct rejections (respond-to-light). The analysis window was the first 150 ms after stimulus onset to minimize any movement effects resulting from licking. For discriminability of pre-stimulus activity between task rules (Fig. 2c), correct trials were split based on block types (respond-to-touch: tactile hits and visual correct rejections; respond-to-light: visual hits and tactile correct rejections). The analysis window was the 100 ms window before stimulus onset. For discriminability of pre-stimulus activity between stimulus types (Fig. 2d), correct trials were split based on stimulus types rather than block types (tactile: tactile hits and tactile correct rejections; visual: visual hits and visual correct rejections). For discriminability of sensory-evoked activity between stimulus types (Fig. 2e), correct trials were split based on stimulus types, and the analysis window was the first 100 ms after stimulus onset rather than before stimulus onset. A Bonferroni corrected 95% confidence interval of AUC was obtained by bootstrap. If this interval did not include the chance level (0.5), it was considered significant.

PSTH-based permutation test

To determine whether water reward affected touch-evoked activity in the cross-modal selection task, we compared the mean PSTHs for tactile hits and for tactile false alarms in which mice licked to the right water port following a tactile stimulus in the respond-to-light blocks (Fig. 1c). For each neuron, the Euclidean distance between the mean PSTHs for tactile hits and tactile false alarms was calculated (0 to 250 ms from stimulus onset). We then performed a permutation test on whether this Euclidean distance was significantly different from zero[41,42]. A p-value was then calculated using the distribution of resampled Euclidean distances. Significance was determined at the alpha = 0.05 level after Bonferroni correction for the number of neurons.

Population decoding analyses

We used linear discriminant analysis (LDA; MATLAB "fitcdiscr") to measure how well population activity from simultaneously recorded neurons could decode (1) task rules (respond-to-touch vs respond-to-light) prior to stimulus delivery (-100 to 0 ms from the stimulus onset), (2) stimulus types (tactile vs visual stimuli) prior to stimulus delivery, and (3) stimulus types after stimulus onset (0 to 100 ms). All correct trials were used and classification accuracy was obtained using ten-fold cross validation (Fig. 3 and Fig. S2c,d). In addition, support vector machines (Fig. S2a; MATLAB "fitcsvm") and Random Forests (Fig. S2b; MATLAB "TreeBagger" with 500 trees) were used to discriminate task rules prior to stimulus delivery. The shuffled data was generated by shuffling the labels for individual trials (e.g. block types).

We also applied LDA to determine how the pre-stimulus states shifted during rule transitions (Fig. 5 and Fig. S4). We used 90% of the correct trials as training data for task rules and the held-out 10% of correct trials to classify trials as having come from respond-to-touch or respond-to-light blocks. We also separately classified trials occurring in the "early transition" and "late transition" periods as having come from one or the other of the block types.

Distance between neural trajectories

We calculated the distance between tHit and tCR trajectories to determine how these trajectories diverged (Fig. 4a,b). For each session, we performed a Principal Components Analysis (PCA) using the trial-averaged tHit and tCR population spike rate responses (-100 to 150 ms from stimulus onset). Population responses for individual tHit and tCR trials were projected onto the top three principal component (PC) space. For each pair of tHit and tCR trials, the Euclidean distances between the neural states of tHit and tCR trajectories at each time point were calculated. The distances between tHit and tCR trajectories were averaged across these pairs in each session.

To investigate the relationship between a difference in pre-stimulus activity and a difference in subsequent sensory-evoked activity, the distances between tHit and tCR trajectories from all recording sessions (total 40 sessions; S1 [10], S2 [8], MM [9], ALM [13]) were ranked based on the distances before stimulus delivery (-100 to 0 ms). The mean tHit-tCR distances after stimulus onset (0 to 150 ms) between the top and bottom 50% groups were compared using a permutation test (Fig. 4c). Specifically, we calculated the Euclidean distance between the mean

tHit-tCR distances for these two groups. The group labels were then randomly shuffled, and new mean tHit-tCR distances of the shuffled groups were obtained. The Euclidean distance between these shuffled mean tHit-tCR distances was calculated. This shuffling procedure was repeated 1,000 times, and then the p value was calculated (one-tailed; null hypothesis: no difference; distance >=0).

Subspace overlap

The subspace overlap between tHit and tCR trials was obtained through their variance alignment (Fig. 4d-f). For each session, the trial-averaged tHit activity was used to perform a PCA (0 to 150 ms from stimulus onset). The trial-averaged tCR activity was projected onto the top three principal component (PC) space ($tCR_{tHit\text{-}subspace}$), and the variance explained was calculated. For normalization, a separated PCA was performed on the trial-averaged tCR activity, and its own ($tCR_{tCR\text{-}subspace}$) variance explained was calculated. The subspace overlap was defined as the ratio of the variance explained of $tCR_{tHit\text{-}subspace}$ to the variance explained of $tCR_{tCR\text{-}subspace}$. We chose the top three PCs because most of the variances of $tHit_{tHit\text{-}subspace}$ (~90%) and $tCR_{tCR\text{-}subspace}$ (~85%) were captured.

To test if the subspace for processing tactile signals significantly changed under different rules, we compared the subspace overlap between tHit and tCR trials with a control group. Specifically, we randomly assigned tactile hit trials into equal sized reference and control groups. The tCR and tHit control group were projected to the PC space of the tHit reference group, and their subspace overlaps were compared (Fig. 4e). To determine if the separation of subspaces began prior to stimulus delivery, pre-stimulus activity in tCR trials was projected to the PC space of the tHit reference group and the subspace overlap was calculated (-100 to 0 ms from stimulus onset). In addition, the subspace overlap could be overestimated when there were only few neurons in a session (low dimensionality). To avoid this issue, sessions having less than ten units were excluded from this analysis.

Stimulus and choice coding dimensions

For each session, *n* simultaneously recorded neurons created an *n* dimensional space. A coding dimension (CD) is defined as an *nx1* vector that maximally separates the neural trajectories for different conditions[47,48] (stimulus CD: tactile vs visual; choice CD: right-lick vs no-lick in a respond-touch block, left-lick vs no-lick in a respond-to-light block). For example, to estimate a stimulus CD in respond-to-touch blocks, we used trial-averaged trajectories for tactile ($\bar{x}_{tactile} = (\bar{x}_{tHit} + \bar{x}_{tMiss})/2$) and visual ($\bar{x}_{visual} = (\bar{x}_{vFA} + \bar{x}_{vCR})/2$) trials and calculated their difference at each time point ($\nu_t = \bar{x}_{tactile} - \bar{x}_{visual}$). We then averaged ν_t during the analysis window (0 to 150 ms from stimulus onset) to obtain the stimulus CD.

To test if stimulus (choice) CDs changed with the task rules, we calculated the dot product between the stimulus (choice) CD in respond-to-touch blocks and the stimulus (choice) CD in respond-to-light blocks. The CDs here are unit vectors, so the magnitude of the dot product ranges from 0 (orthogonal) to 1 (aligned).

Stimulus sensitivity

For the cross-modal sensory selection task, the detection sensitivity for tactile stimuli was calculated as the difference of tactile hit rate and visual false alarm rate during the respond-to-touch blocks. The tactile hit rate was the probability of licking right in response to tactile stimuli, and the visual false alarm rate was the probability of licking right in response to visual stimuli. Correspondingly, the detection sensitivity for visual stimuli was determined by the difference of visual hit rate and tactile false alarm rate during the respond-to-light blocks. The visual hit rate was the probability of licking left in response to visual stimuli, and the tactile false alarm rate was the probability of licking left in response to tactile stimuli.

For the tactile detection task, the detection sensitivity for tactile stimuli was calculated as the difference of hit rate and false alarm rate. The hit rate was the probability of licking in the stimulus trials (Go trials), and the false alarm rate was the probability of licking in the no-stimulus trials (NoGo trials).

Statistics

We report data as mean ± standard error of the mean (s.e.m.) except where noted. Statistical tests were two-tailed unless otherwise noted. We made the Bonferroni correction for multiple comparisons across neurons in each cortical area (Fig. 1h and 2c-e).

We calculated confidence intervals using a nonparametric hierarchical bootstrap method[90] to simulate the data generation process and to incorporate variability at different levels including mice, sessions, neurons, and trial types. For population decoding analysis (Fig. 3-5 and Fig. S2-4), statistical tests were performed across sessions (e.g., a mean classification accuracy for task rules across sessions). For behavioral analysis during optogenetic inhibition (Fig. 6 and Fig. S5,6), statistical tests were performed across mice (e.g., a mean tactile sensitivity across mice).

Data and code availability

Data and MATLAB scripts used to analyze the data are available from the corresponding author upon request.

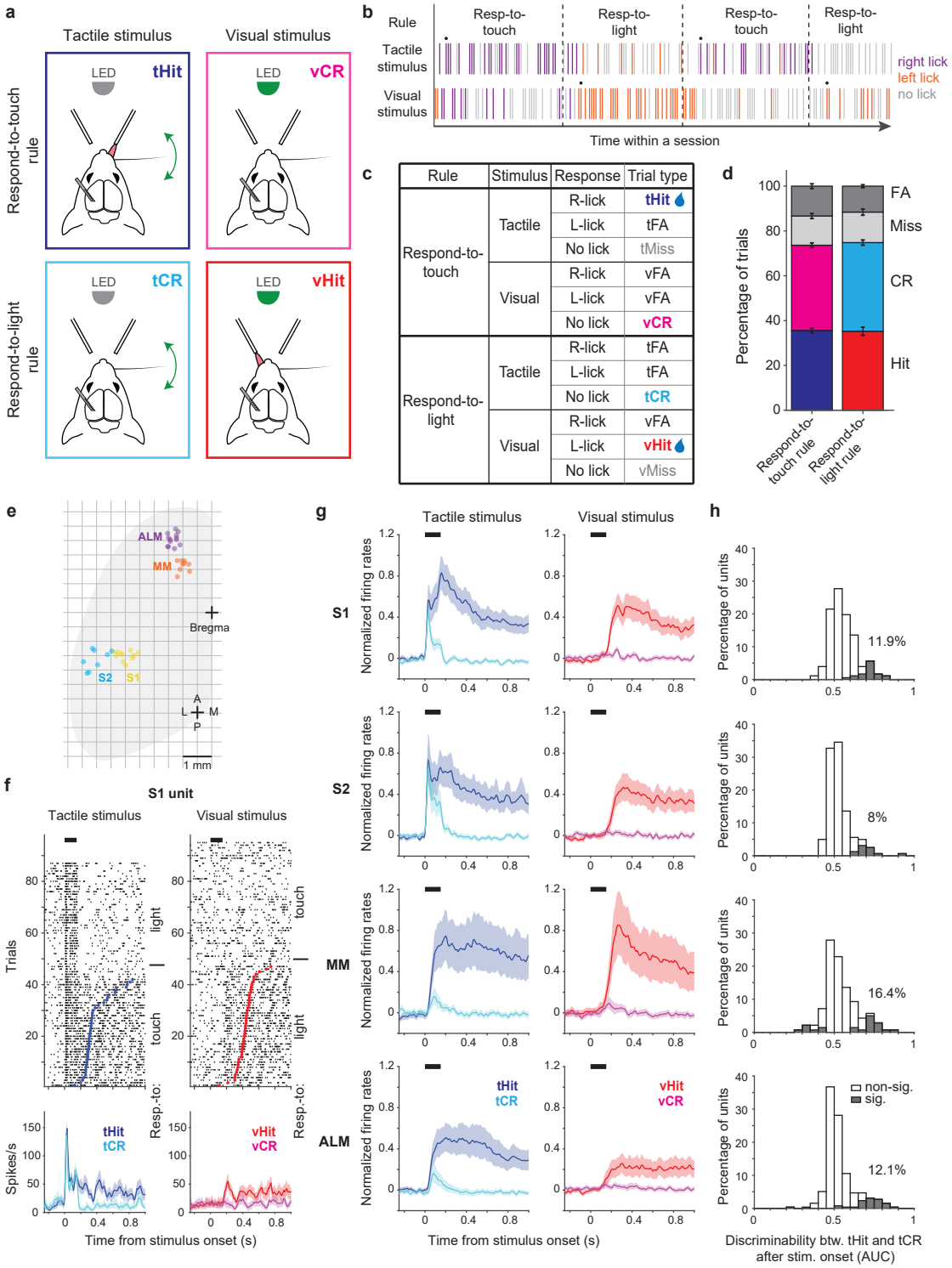

Rule	Stimulus	Response	Trial type
Respond-to-touch	Tactile	R-lick	tHit
		L-lick	tFA
		No lick	tMiss
	Visual	R-lick	vFA
		L-lick	vFA
		No lick	vCR
Respond-to-light	Tactile	R-lick	tFA
		L-lick	tFA
		No lick	tCR
	Visual	R-lick	vFA
		L-lick	vHit
		No lick	vMiss

Figure 1 | Touch-evoked activity of individual neurons is modulated by task rules.

a, Schematic of the cross-modal sensory selection task. Tactile and visual stimuli were associated with water reward during the respond-to-touch and respond-to-light rules, respectively. Mice were trained to lick to the right reward port after a tactile stimulus during the respond-to-touch rule, and lick to the left reward port after a visual stimulus during the respond-to-light rule. Mice withheld licking after a reward irrelevant stimulus (tactile stimulus during the respond-to-light rule or visual stimulus during the respond-to-touch rule). **b**, Example behavioral session. Tactile and visual trials were randomly interleaved. Respond-to-touch and respond-to-light rules alternated in different blocks of trials during a behavioral session (~60 trials/block). The mouse adaptively changed its stimulus-response strategies based on the task rules. Each bar represents a trial and colors indicate lick responses (right lick: purple; left lick: orange; no lick: gray). A drop of water was delivered to the new reward port on the 9th trial (black dot) to cue mice to the rule switch. **c**, Task design and trial outcomes. Correct licking responses were hits, and correct withholding of responses were correct rejections (CR). Failed responses were misses, and incorrect licking responses were false alarms (FA). Two sensory modalities and four types of trial outcomes comprise eight trial types. **d**, The fractions of trial outcomes were similar between the respond-to-touch and respond-to-light rules (touch vs light: hit (36±1% vs 35±2%); correct rejection (38±1% vs 40±1%); miss (13±1% vs 14±1%); false alarm (13±1% vs 12±1%)). The behavioral performance was ~75% correct for both rules (touch: 74±1%, light: 75±1%). Means ± SEM; n = 12 mice.

e, Reconstructed locations of silicon probes. S1: primary somatosensory cortex (6 mice, 10 sessions). S2: secondary somatosensory cortex (5 mice, 8 sessions). MM: medial motor cortex (7 mice, 9 sessions). ALM: anterolateral motor cortex (8 mice, 13 sessions). **f**, Raster plots (top) and trial-averaged activity (bottom) of an example S1 unit. Correct tactile (left) and visual (right) trials were sorted by rule and response (tactile hit (tHit, blue); tactile correct rejection (tCR, cyan); visual hit (vHit, red); visual correct rejection (vCR, magenta)). Dots indicate the first lick in hit trials. Thick black bars show the stimulus delivery window. Error shading: bootstrap 95% confidence interval [CI]. **g**, Normalized activity (z-score) across the population of recorded neurons in S1 (177 neurons), S2 (162 neurons), MM (140 neurons), and ALM (256 neurons). Error shading: bootstrap 95% CI. **h**, Distribution of tHit and tCR discriminability for individual neurons. Discriminability of tHits and tCRs was defined as the ability of an ideal observer to discriminate tHits from tCRs on a trial-by-trial basis (average AUC; 0 to 150 ms; 10 ms bins). Approximately 5 to 20 percent of neurons showed significant difference between tHit and tCR responses (gray area; Bonferroni corrected 95% CI does not include 0.5) in S1 (11.9%), S2 (8%), MM (16.4%) and ALM (12.1%).

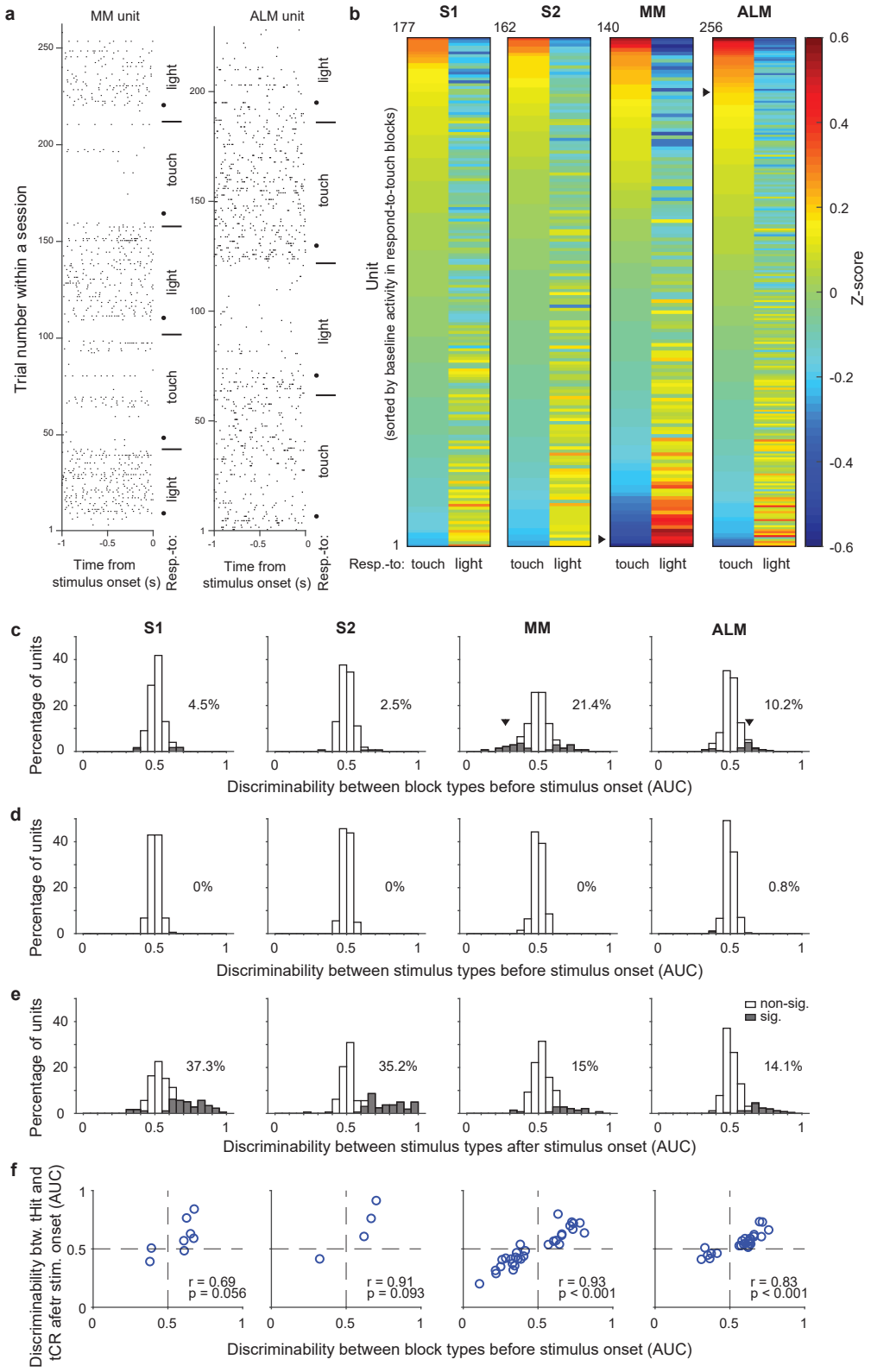

Figure 2 | Single-unit activity before stimulus delivery reflects task rules.

a, Raster plots for example units from MM (left) and ALM (right). Neural activity before stimulus delivery (-1 to 0 seconds from stimulus onset) changed across blocks within a session. Horizontal lines show block transitions and black dots indicate switch cues. **b**, Heatmap of normalized (z-scored) pre-stimulus activity (-100 to 0 ms) across correct trials in respond-to-touch and respond-to-light blocks for units in S1 (n=177), S2 (n=162), MM (n=140), and ALM (n=256). Right-pointing triangles label example units in **a**. **c**, Distribution of respond-to-touch and respond-to-light discriminability for individual neurons. The respond-to-touch and respond-to-light discriminability was measured by the ability of an ideal observer to discriminate respond-to-touch from respond-to-light pre-stimulus mean activity (-100 to 0 ms) on a trial-by-trial basis (AUC). The percentages of units showing significant discriminability (gray areas: Bonferroni corrected 95% CI of AUC did not include 0.5) were higher in motor cortical regions (MM: 21.4%; ALM: 10.2%) than in sensory cortical regions (S1: 4.5%; S2: 2.5%). Downward-pointing triangles label example units in **a**. **d**, Distribution of stimulus discriminability (tactile vs visual stimuli) for individual neurons during the pre-stimulus-onset window (-100 to 0 ms). Almost no units show significant stimulus discriminability before the stimulus onset (S1: 0%; S2: 0%; MM: 0%; ALM: 0.8%). **e**, Same as **d** but for the post-stimulus-onset window (0 to 100 ms). A large percentage of units show significant stimulus discriminability after the stimulus onset (S1: 37.3%, S2: 35.2%, MM 15%, and ALM 14.1%). **f**, Relationship between block-type discriminability before stimulus onset and tHit-tCR discriminability after stimulus onset for units showing significant block-type discriminability prior to the stimulus.

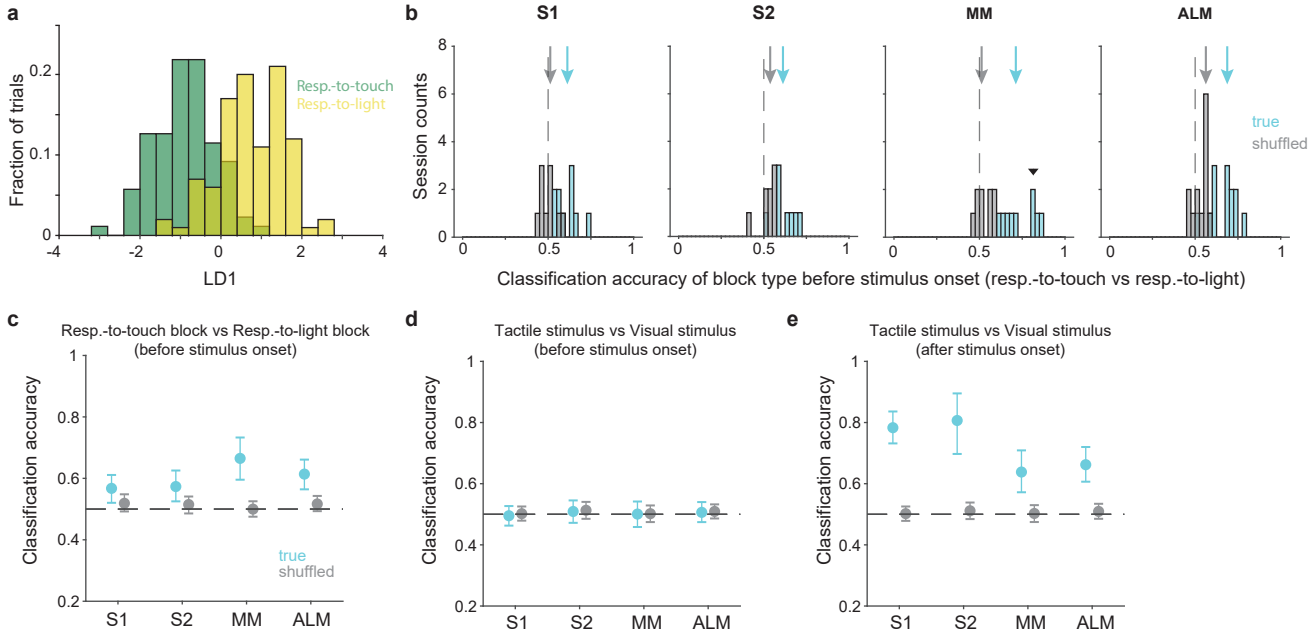

Figure 3 | Pre-stimulus states of neural populations are rule-dependent.

a, Decoding of task rule (respond-to-touch vs respond-to-light) through linear discriminant analysis (LDA) for an example session. Pre-stimulus population activity (MM; 21 neurons; -100 to 0 ms from stimulus onset) in respond-to-touch (green) and respond-to-light (yellow) blocks were projected onto the first linear discriminant (LD1). This plot shows the histogram of the projections onto the LD1 axis. **b**, Distribution of classification accuracy of task rule (respond-to-touch vs respond-to-light) based on pre-stimulus activity for simultaneously recorded neurons in each session (S1:10 sessions; S2: 8 sessions; MM: 9 sessions; ALM: 13 sessions). The true (cyan) data showed better classification accuracy compared with the shuffled (gray) data (medians of classification accuracy [true vs shuffled]: S1 [0.61 vs 0.5]; S2 [0.62 vs 0.53]; MM [0.7 vs 0.52]; ALM [0.68 vs 0.55]). Arrows show classification accuracy medians. Dashed lines indicate the chance level (0.5). The downward-pointing triangle shows the example session in **a**. **c**, Session-averaged classification accuracy of task rules based on pre-stimulus population activity in S1 (95% CI of true (cyan) and shuffled (gray) data: true [0.52,0.61], shuffled [0.49,0.55]), S2 (true [0.53,0.63], shuffled [0.49, 0.54]), MM (true [0.60,0.73], shuffled [0.48, 0.53]) and ALM (true [0.56,0.66], shuffled [0.49, 0.54]). Error bars show bootstrap 95% CI. **d**, Same as **c** but for the classification accuracy of stimulus types. **e**, Same as **c** but for the classification accuracy of stimulus types based on population activity after stimulus onset (0 to 100 ms).

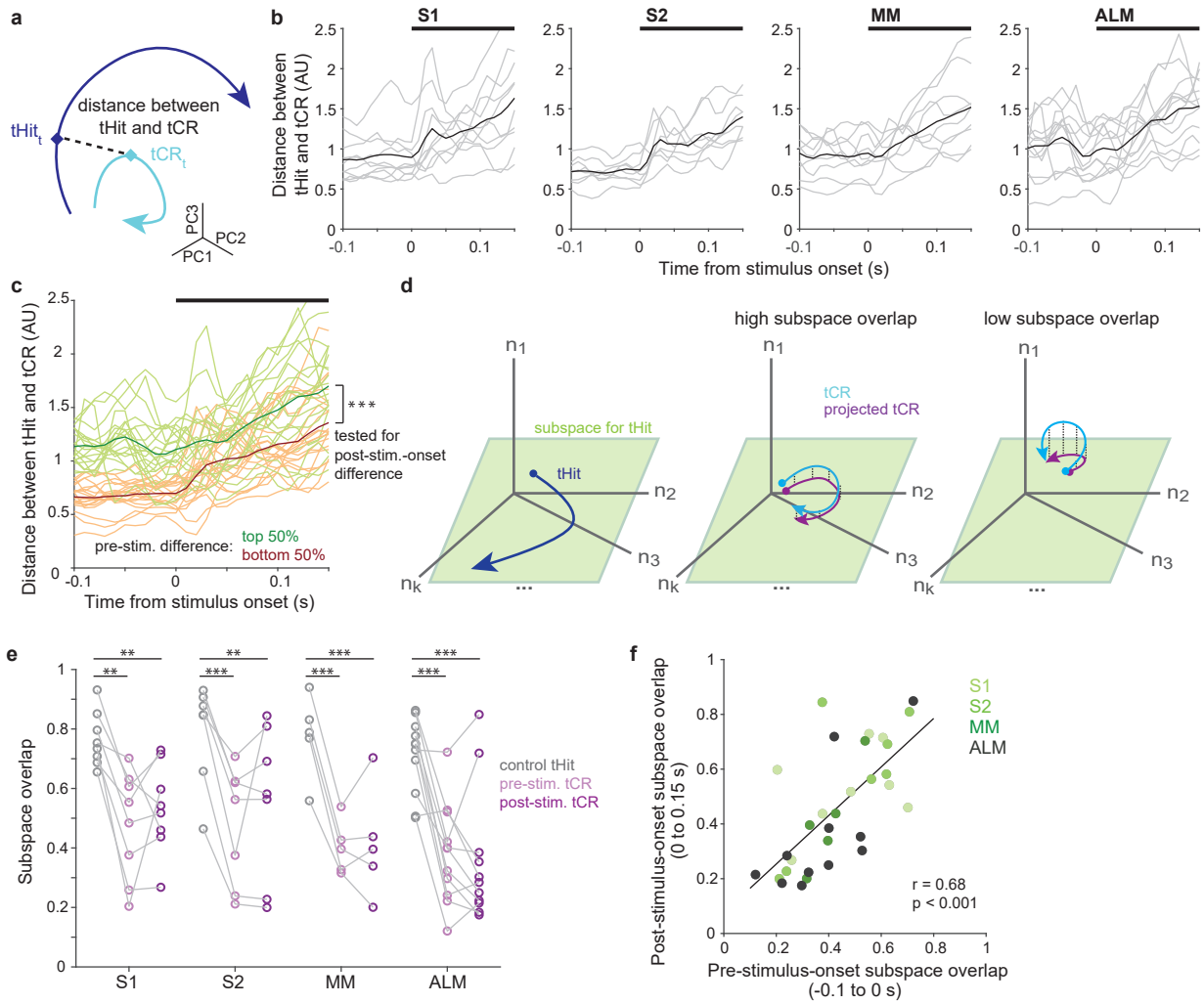

Figure 4 | Pre-stimulus states predict subsequent tactile processing.

a, Schematic of distance (dashed line) between tHit (blue) and tCR (cyan) trajectories. **b**, Distance between tHit and tCR trajectories in S1, S2, MM and ALM. **c**, Distance between tHit and tCR trajectories. Traces show individual sessions (n = 40) pooled across areas and were sorted and labeled based on the distance prior to the stimulus (top 50%: green; bottom 50%: orange). The post-stimulus-onset distance was larger in the top 50% group than the bottom 50% group (permutation test, $p < 0.001$). In **b** and **c**, thick black bars show periods of stimulus delivery. **d**, Schematic of the subspace overlap between tHit and tCR. A subspace (green parallelogram) for population activity of tHit (blue) is in a high dimensional neural state space (left panel). If the subspaces of tHit and tCR are aligned, the tHit subspace could explain much of the variance of tCR (high subspace overlap; middle panel). That is, the projection of tCR onto the tHit subspace (purple) preserves much of the variance of tCR (cyan). If the subspaces of tHit and tCR are unaligned, the projection of tCR onto the tHit subspace preserves little of the variance of tCR (right panel). **e**, Subspace overlap for control tHit (gray), pre- (light purple) and post- (dark purple) stimulus-onset tCR trials in the somatosensory and motor cortical areas. Each circle is a subspace overlap of a session (S1: 8 sessions; S2: 7 sessions; MM: 5 sessions; ALM: 11 sessions). Significance: ** for $p<0.01$, *** for $p<0.001$. **f**, Relationship between pre- and post-stimulus-onset subspace overlaps. The subspace overlaps between tHit and tCR trials, calculated during pre- and post-stimulus-onset periods, were correlated (Pearson correlation, $r=0.68$, $p < 0.001$; linear regression (black line); 31 sessions).

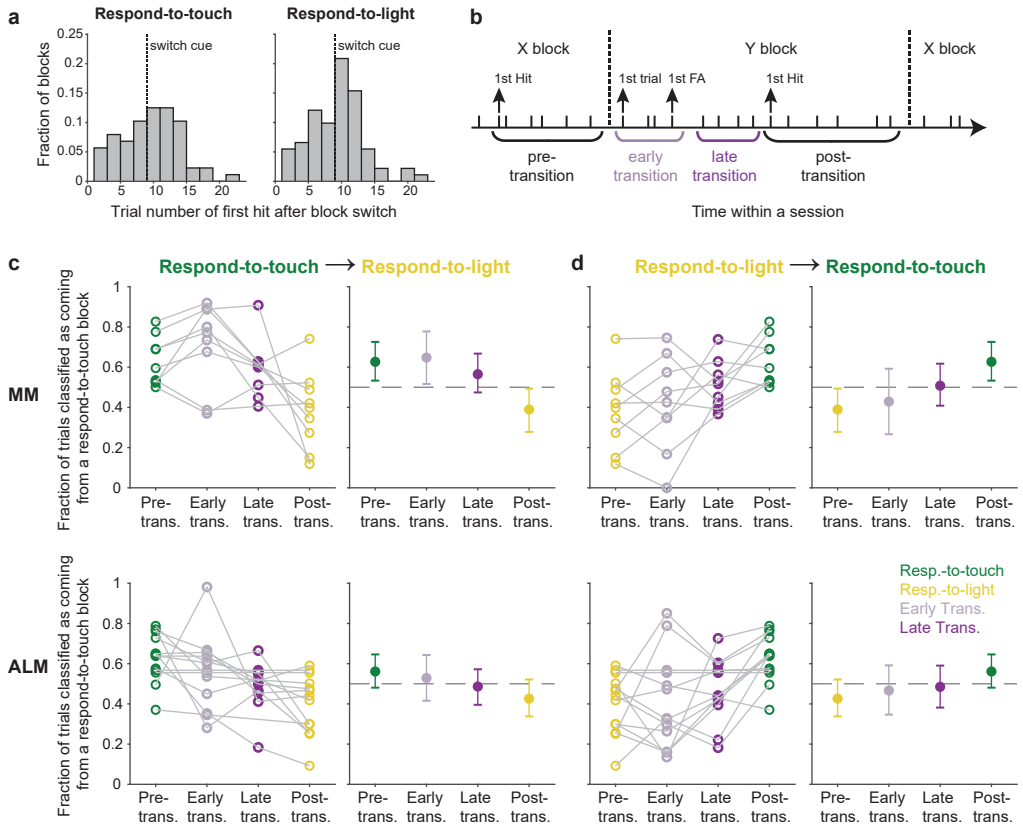

Figure 5 | Pre-stimulus states of the motor cortical areas track behavioral rule switching.

a, Histogram showing the distribution of the trial number of the first hit after block switch. Most first hits in respond-to-touch (left) and respond-to-light (right) blocks occurred before or immediately after the switch cue (dashed line). **b**, Schematic of rule transition in the cross-modal selection task. A transition period was defined as spanning from the first trial after the block switch until the first hit trial of that block. “Early” and “late” transitions were separated by the first false alarm trial of that block. **c**, Fraction of trials classified as coming from a respond-to-touch block based on the pre-stimulus population state, for trials occurring in different periods (see **b**) relative to respond-to-touch → respond-to-light transitions. For MM (top row) and ALM (bottom row), progressively fewer trials were classified as coming from the respond-to-touch block as analysis windows shifted later relative to the rule transition. (Left panels: individual sessions; right panels: mean ± 95% CI across 9 (MM) or 12 (ALM) sessions. Dash lines are chance levels (0.5). **d**, Same as **c** but for respond-to-light → respond-to-touch transitions.

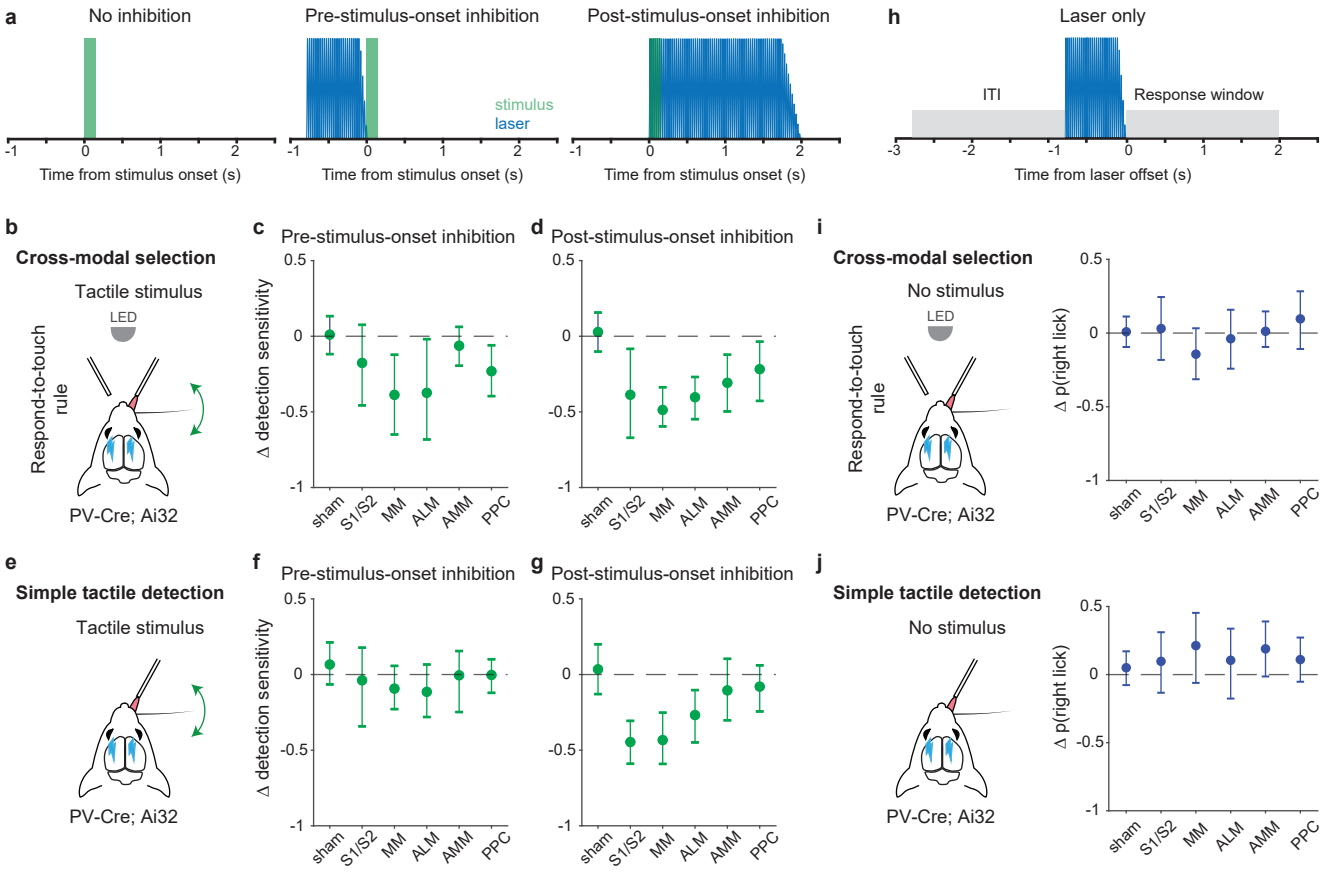

Figure 6 | Inhibition of pre-stimulus states in the motor cortex impairs rule-dependent tactile detection.

a, Schematic of inhibition conditions for stimulus trials. Sessions comprised 80% stimulus trials and 20% laser only trials (see **h**). In 15% of the stimulus trials, optogenetic inhibition occurred before tactile or visual stimuli (middle, -0.8 to 0 s from stimulus onset) to suppress pre-stimulus activity in the targeted cortical area. In another 15% of stimulus trials, optogenetic inhibition began simultaneously with the stimulus onset (right, 0 to 2 s from stimulus onset) in order to suppress sensory-evoked activity. **b-d**, Changes in detection sensitivity for tactile stimuli during respond-to-touch blocks in the cross-modal selection task when each cortical area was optogenetically inhibited. For pre-stimulus-onset inhibition (**c**), detection sensitivity decreased when MM and ALM but not S1 and S2 were suppressed. For post-stimulus-onset inhibition (**d**), the detection sensitivity decreased when sensory and motor cortical regions were suppressed. S1/S2: 4 mice, 10 sessions; MM: 4 mice, 11 sessions; ALM: 4 mice, 10 sessions. Sham: 7 mice, 28 sessions. AMM: anteromedial motor cortex, 7 mice, 21 sessions. PPC: posterior parietal cortex, 7 mice, 21 sessions. **e-g**, Same as **b-d** but for a simple tactile detection task (not cross-modal selection task). Detection sensitivity for tactile stimuli was reduced when the sensory (S1 and S2) and motor (MM and ALM) cortical areas were inhibited during the post-stimulus-onset window (**g**) but not during the pre-stimulus-onset window (**f**). Sham: 5 mice, 9 sessions; S1/S2: 3 mice, 3 sessions; MM: 3 mice, 5 sessions; ALM: 3 mice, 4 sessions; AMM: 3 mice, 4 sessions; PPC: 3 mice, 4 sessions. Means ± 95% CI. **h**, Schematic of inhibition conditions for “laser only” trials. The probability of licking during the response window (0 to 2 s from laser offset) was compared with the probability of licking during the intertrial interval (ITI, -2 to 0 s from laser onset). **i**, Changes in the probability of right licks within the laser only trials during respond-to-touch blocks in the cross-modal selection task. **j**, Changes in the probability of right licks within the laser only trials in the simple tactile detection task. Error bars show bootstrap 95% CI.

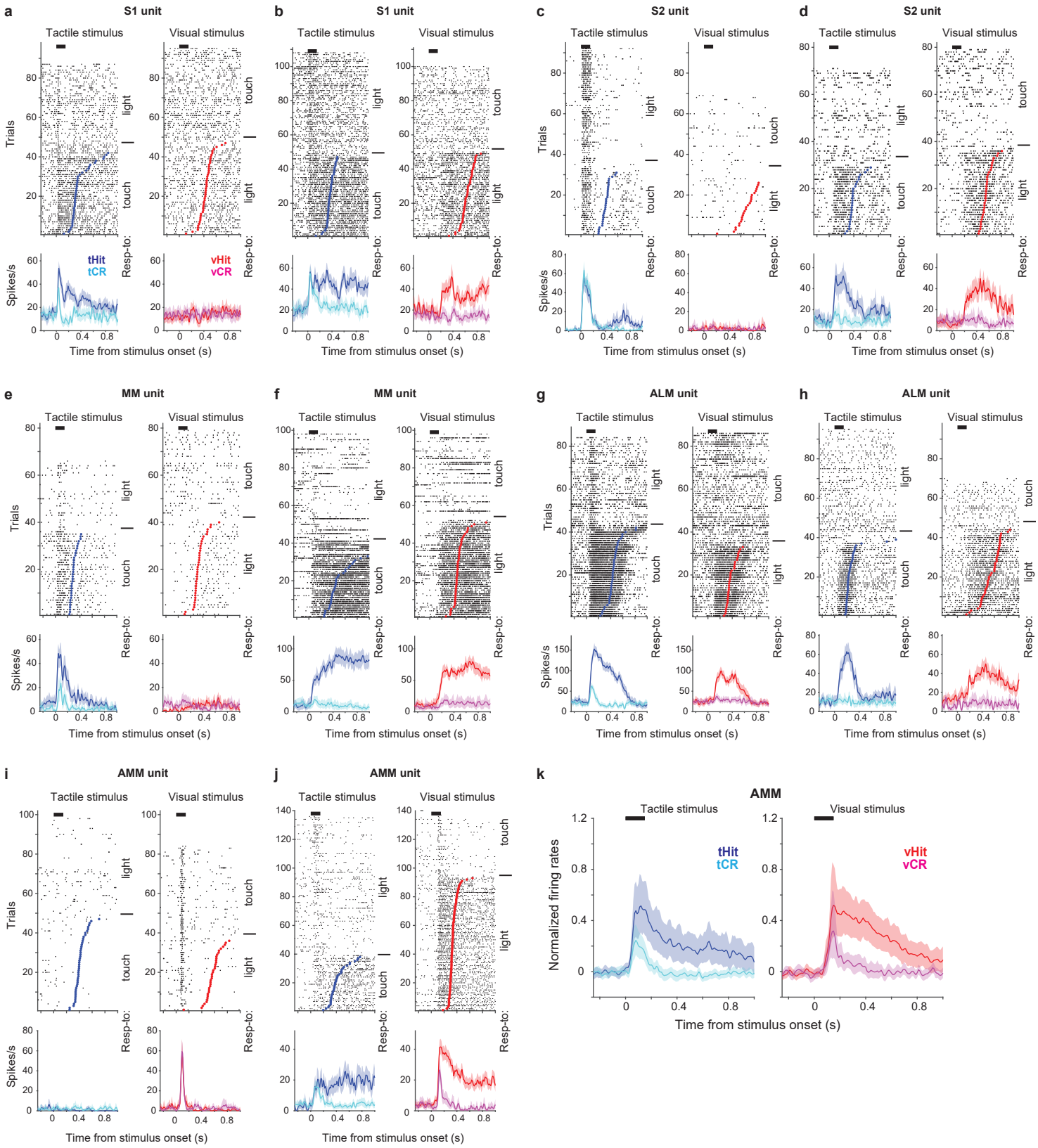

Figure S1 | Additional examples of single-unit responses during the cross-modal selection task.

a, **b**, Raster plots (top) and trial-averaged activity (bottom) of two example S1 units. Correct tactile (left) and visual (right) trials were grouped by rules and responses (tactile hit (tHit, blue); tactile correct rejection (tCR, cyan); visual hit (vHit, red); visual correct rejection (vCR, magenta)). Dots indicate the first lick in hit trials. Thick black bars show periods of stimulus delivery. Error shading shows bootstrap 95% CI. **c-j**, Same as **a** and **b** but for example units from S2 (**c, d**), MM (**e, f**), ALM (**g, h**) and AMM (the anteromedial part of the motor cortex; **i, j**). **k**, Normalized activity (z-score) across the population of recorded neurons in AMM (110 neurons). Error shading: bootstrap 95% CI.

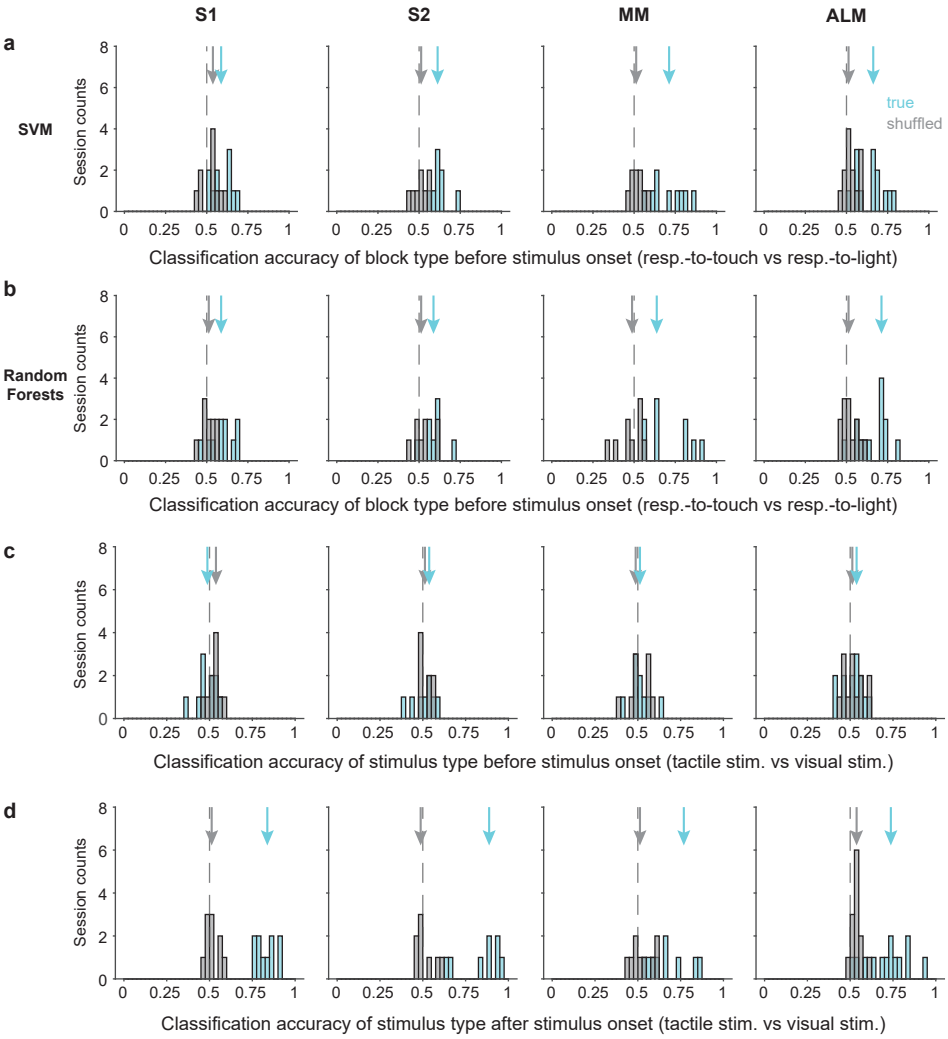

Figure S2 | Classification accuracy for task rules and stimulus types.

a, Distribution of classification accuracy of task rule (respond-to-touch vs respond-to-light) based on pre-stimulus population activity (-100 to 0 ms from stimulus onset) using a support vector machine (SVM). Arrows show classification accuracy medians of true (cyan) and shuffled (gray) data. Dashed lines indicate the chance level (0.5). **b**, Same as a but using a Random Forests classifier. **c**, Distribution of classification accuracy of stimulus types (tactile stimulus vs visual stimulus) based on pre-stimulus population activity using LDA. **d**, Same as **c** but based on population activity after stimulus onset (0 to 100 ms from stimulus onset).

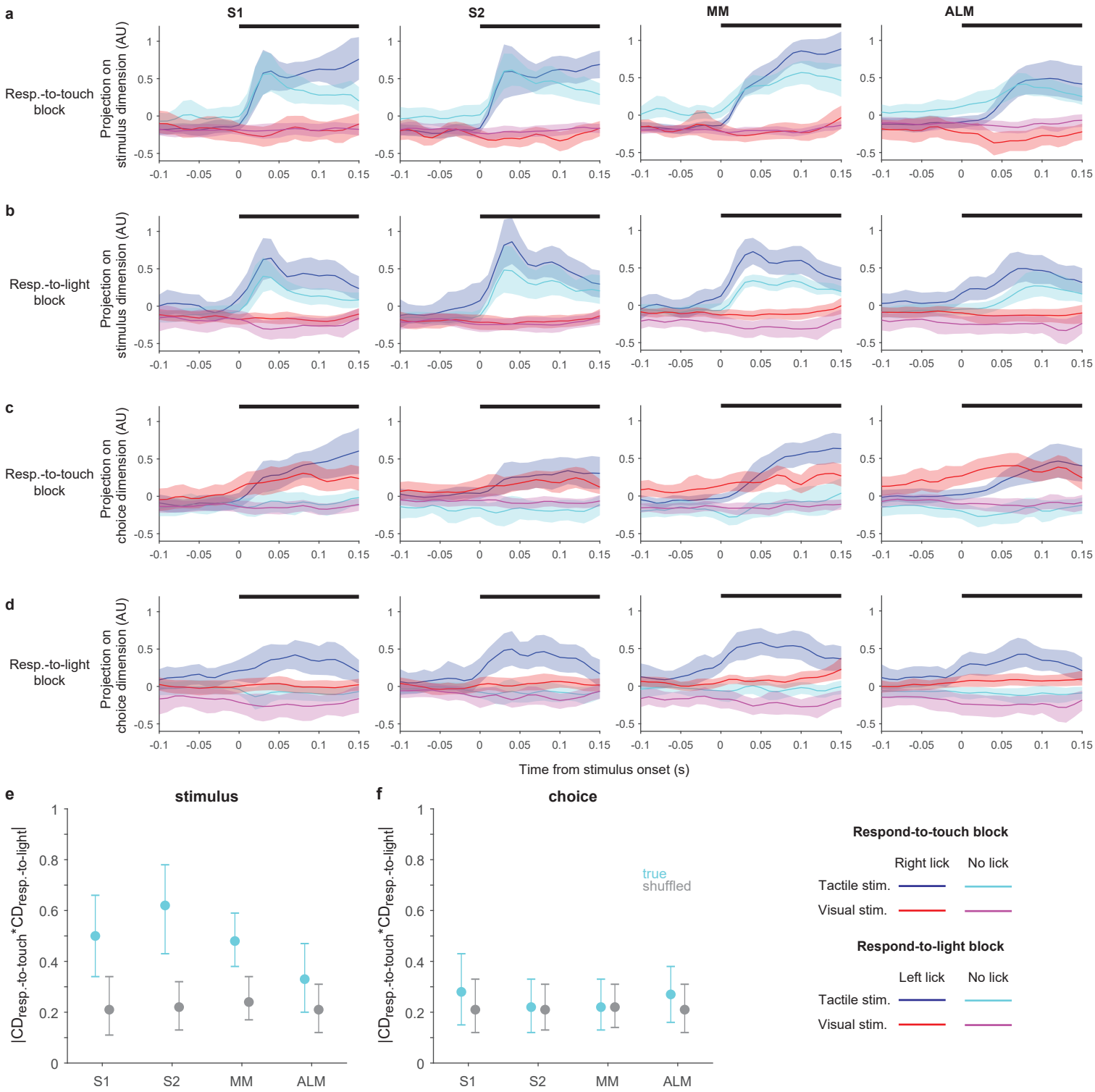

Figure S3 | Stimulus and choice coding dimensions in respond-to-touch and respond-to-light blocks.

a, Population activity projected on the stimulus coding dimension (CD) in respond-to-touch blocks. Two stimulus types and two behavioral responses compose four conditions (tactile-right-lick: blue; tactile-no-lick: cyan; visual-right-lick: red; visual-no-lick: magenta). Thick black bars (on the top of each panel) show periods of stimulus delivery (0 to 150 ms). Error shading: bootstrap 95% CI. **b**, Population activity projected on the stimulus coding dimension in respond-to-light blocks. Two stimulus types and two behavioral responses compose four conditions (tactile-left-lick: blue; tactile-no-lick: cyan; visual-left-lick: red; visual-no-lick: magenta). **c**, Same as **a** but for choice coding dimensions. **d**, Same as **b** but for choice coding dimensions. **e**, Magnitude of dot product between the stimulus CDs in respond-to-touch and respond-to-light blocks. Means ± 95% CI from bootstrapping. **f**, Same as **e** but for choice CDs.

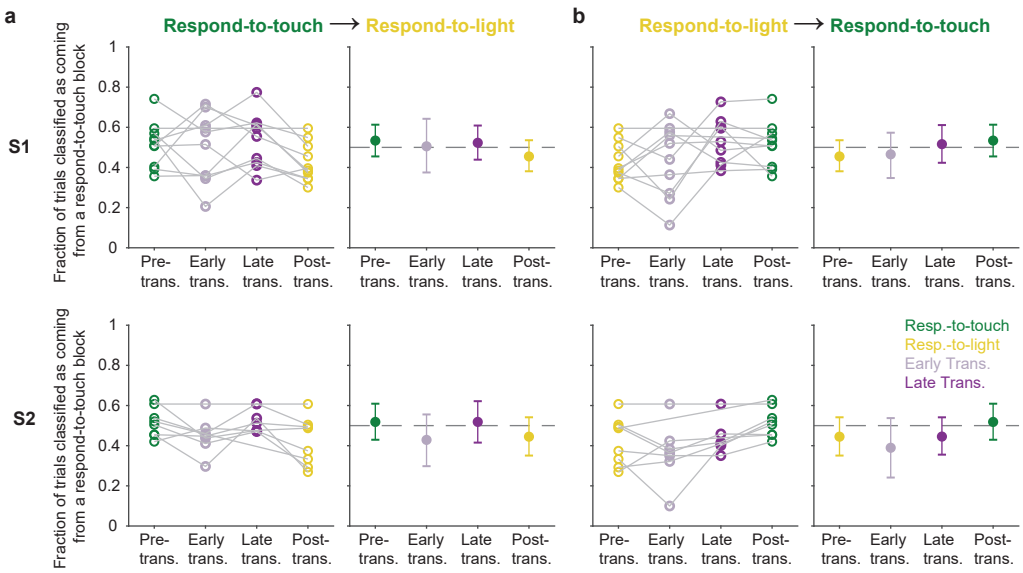

Figure S4 | Pre-stimulus states of neural populations in the sensory cortex during rule transitions.

a, Fraction of trials classified as coming from a respond-to-touch block based on the pre-stimulus population state, for trials occurring in different periods (see Fig. 5b) relative to respond-to-touch → respond-to-light transitions. Top row: S1; bottom row: S2. Left panels: individual sessions; right panels: mean ± 95% CI across 10 (S1) or 8 (S2) sessions. **b**, Same as a but for respond-to-light → respond-to-touch transitions.

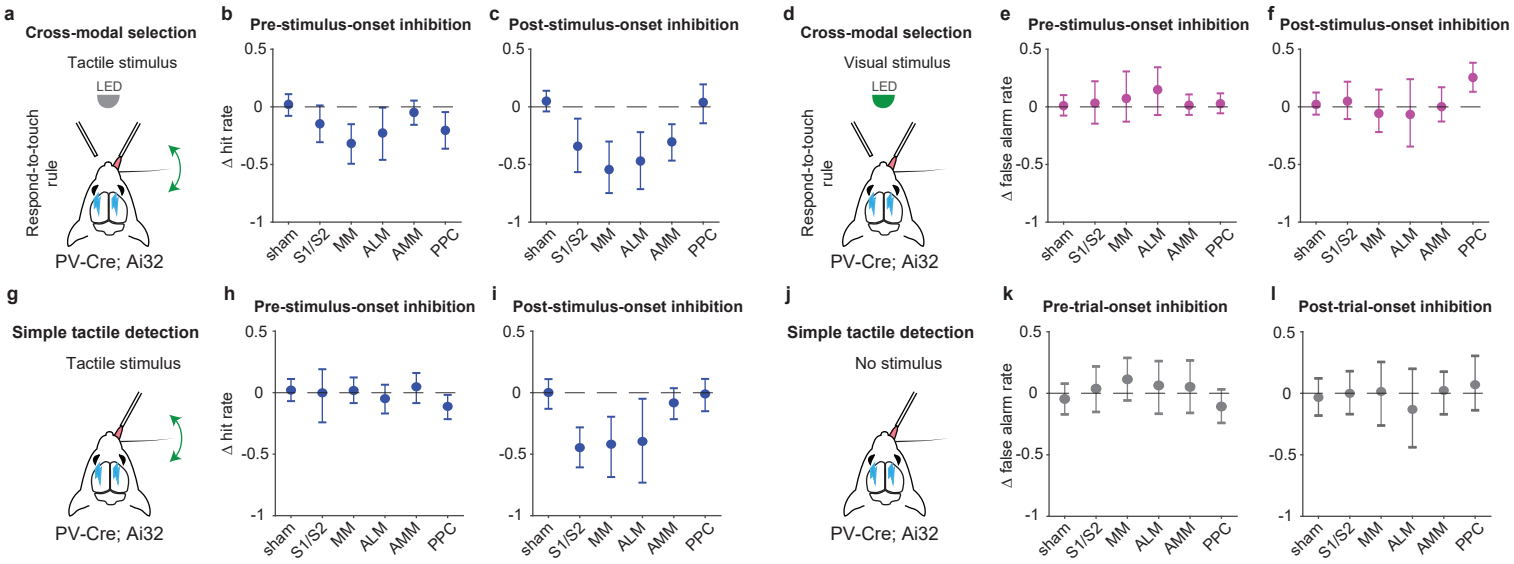

Figure S5 | Hit and false alarm rates during the inhibition of population states in the dorsal cortex.

a, Schematic of inhibition within tactile stimulus trials during respond-to-touch blocks in the cross-modal selection task. **b**, Changes in tactile hit rate when each cortical area was optogenetically inhibited before stimulus onset. The tactile hit rate is the probability of right licks for tactile stimuli during respond-to-touch blocks. S1/S2: 4 mice, 10 sessions; MM: 4 mice, 11 sessions; ALM: 4 mice, 10 sessions. Sham: 7 mice, 28 sessions. AMM: 7 mice, 21 sessions. PPC: 7 mice, 21 sessions. Means ± 95% CI from bootstrapping. **c**, Same as **b** but for inhibition after stimulus onset. **d**, Schematic of inhibition within visual stimulus trials during respond-to-touch blocks in the cross-modal selection task. **e**, Changes in visual false alarm rate when each cortical area was optogenetically inhibited before stimulus onset. The false alarm rate is the probability of right licks for visual stimuli during respond-to-touch blocks. **f**, Same as **e** but for inhibition after stimulus onset. **g**, Schematic of inhibition within tactile stimulus trials in the tactile detection task. **h**, Changes in tactile hit rate when each cortical area was optogenetically inhibited before stimulus onset. The tactile hit rate is the probability of right licks for tactile stimuli in the tactile detection task. Sham: 5 mice, 9 sessions; S1/S2: 3 mice, 3 sessions; MM: 3 mice, 5 sessions; ALM: 3 mice, 4 sessions; AMM: 3 mice, 4 sessions; PPC: 3 mice, 4 sessions. Means ± 95% CI from bootstrapping. **i**, Same as **h** but for inhibition after stimulus onset. **j,** Schematic of inhibition when there was no stimulus in the tactile detection task. **k**, Changes in false alarm rate when each cortical area was optogenetically inhibited before trial onset. The false alarm rate is the probability of right licks when there was no stimulus. **l**, Same as **k** but for inhibition after trial onset.

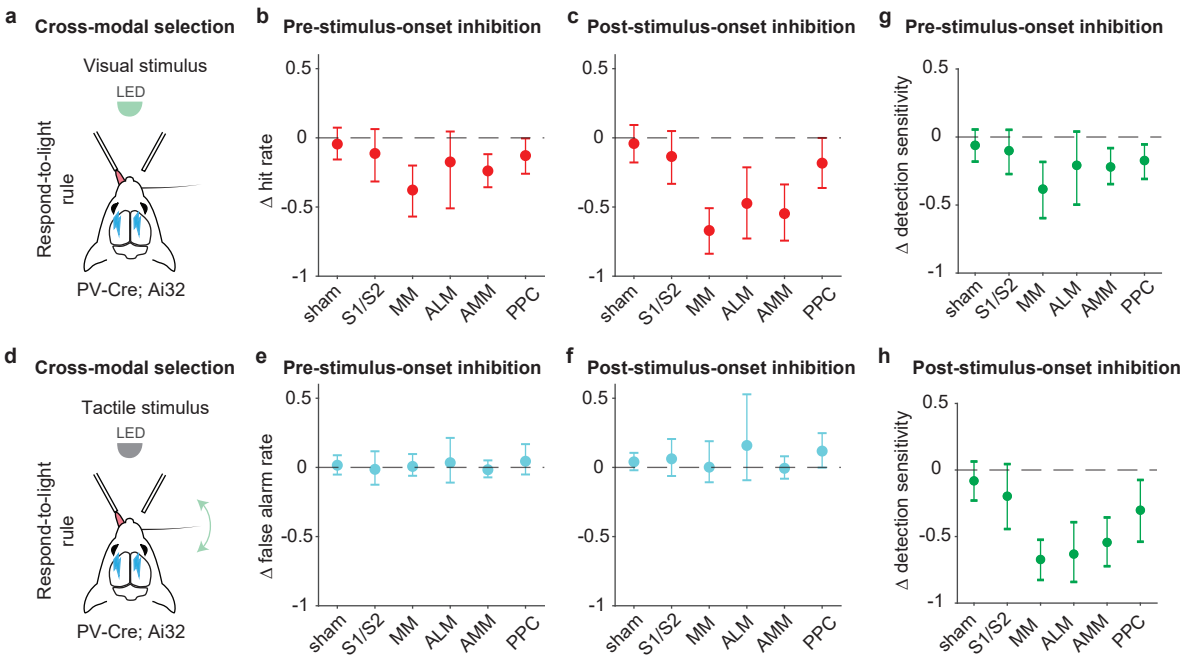

Figure S6 | Inhibition of pre-stimulus states in the medial motor cortex impairs rule-dependent visual detection.

a, Schematic of inhibition within visual stimulus trials during the respond-to-light blocks in the cross-modal selection task. **b**, Changes in visual hit rate when each cortical area was optogenetically inhibited before stimulus onset. The visual hit rate is the probability of left licks for visual stimuli during respond-to-light blocks. S1/S2: 4 mice, 10 sessions; MM: 4 mice, 11 sessions; ALM: 4 mice, 10 sessions. Sham: 7 mice, 28 sessions. AMM: 7 mice, 21 sessions. PPC: 7 mice, 21 sessions. Means ± 95% CI from bootstrapping. **c**, Same as **b** but for inhibition after stimulus onset. **d**, Schematic of inhibition within tactile stimulus trials during respond-to-light blocks in the cross-modal selection task. **e**, Changes in tactile false alarm rate when each cortical area was optogenetically inhibited before stimulus onset. The false alarm rate is the probability of left licks for tactile stimuli during respond-to-light blocks. **f**, Same as **e** but for inhibition after stimulus onset. **g**, Changes in detection sensitivity for visual stimuli when each cortical area was inhibited before stimulus onset. The detection sensitivity for visual stimuli was determined by the difference of visual hit rate and tactile false alarm rate during respond-to-light blocks. **h**, Same as **g** but for inhibition after stimulus onset.

Animal ID	Genotype	Sex	Date of Birth	Test Session Dates	Figure Appearances
EF0147	Emx-Cre; Ai32	male	180627	190204 - 190206	Fig. 1d,e,g,h; 2b-f; 3b-e; 4; 5; S1h,k; S2; S3; S4
EF0148	Emx-Cre; Ai32	male	180627	190228 - 190305	Fig. 1d,e,g,h; 2b-f; 3b-e; 4; 5; S1c,i,k; S2; S3; S4
EF0150	Emx-Cre; Ai32	male	180627	190223 - 190318	Fig. 1d,e,g,h; 2b-f; 3b-e; 4; 5; S1j,k; S2; S3; S4
EF0151	Emx-Cre; Ai32	male	180627	190506	Fig. 1d,e,g,h; 2; 3b-e; 4; 5; S1g,k ; S2; S3; S4
YT053	PV-Cre; Ai32	male	180211	181115 - 181207	Fig 6c,d,i; S5b,c,e,f; S6
JL005	VGAT-ChR2	male	181121	190716 - 190723	Fig. 1d,e,g,h; 2b-f; 3b-e; 4; 5; S1e,k; S2; S3; S4
YT071	VGAT-ChR2	male	180726	190721 - 190722	Fig. 1d,e,g,h; 2; 3b-e; 4; 5; S1f,k; S2; S3; S4
YT080	PV-Cre; Ai32	male	181112	190503 - 190514; 190827 - 190828	Fig. 1d,e,g,h; 2b-f; 3b-e; 4; 5; 6c,d,i; S1k; S2; S3; S4; S5b,c,e,f; S6
YT081	PV-Cre; Ai32	male	181112	190418 - 190505; 190826 - 190908	Fig. 1d,e,g,h; 2b-f;3; 4; 5; 6c,d,i; S1b,k; S2; S3; S4; S5b,c,e,f; S6
YT083	PV-Cre; Ai32	female	190401	191205 - 200108; 200123	Fig. 1d,e,g,h; 2b-f; 3b-e; 4; 5; 6c,d,i; S1k; S2; S3; S4; S5b,c,e,f; S6
YT084	PV-Cre; Ai32	female	190620	191020 - 200103; 200124 - 200210	Fig. 1b,d-h; 2b-f; 3b-e; 4; 5; 6c,d,i; S1a,k; S2; S3; S4; S5b,c,e,f; S6
YT085	PV-Cre; Ai32	male	190620	191205 - 200108; 200308 - 200320	Fig. 1d,e,g,h; 2b-f; 3b-e; 4; 5; 6c,d,i; S1d,k; S2; S3; S4; S5b,c,e,f; S6
YT086	PV-Cre; Ai32	male	190620	191205 - 200110; 200314 - 200320	Fig. 1d,e,g,h; 2b-f; 3b-e; 4; 5; 6c,d,i; S1k; S2; S3; S4; S5b,c,e,f; S6
YT091	PV-Cre; Ai32	male	200830	201124 - 201211	Fig 6f,g,j; S5h,l,k,l
YT092	PV-Cre; Ai32	female	200830	201126 - 201214	Fig 6f,g,j; S5h,l,k,l
YT093	PV-Cre; Ai32	male	200919	210102 - 210106	Fig 6f,g,j; S5h,l,k,l
YT094	PV-Cre; Ai32	male	200919	201228 - 210103	Fig 6f,g,j; S5h,l,k,l
YT095	PV-Cre; Ai32	female	200919	201230 - 210116	Fig 6f,g,j; S5h,l,k,l

TABLE 1. Experimental subjects.
Tabulated metadata for each mouse, including appearances in each figure.